Norwegian University of Life Sciences

Master Thesis 2019 60 ECTS

Faculty of Environmental Sciences and Natural Resource Management (MINA)

The transfer of radiocesium in coastal waters

- **Radiocesium tracer to investigate mixing zone processes in brackish waters**

Birgitte Brockstedt Kvamme

Radioecology

THE TRANSFER OF RADIOCESIUM IN COASTAL WATERS

Radiocesium tracer to investigate mixing zone processes in brackish waters

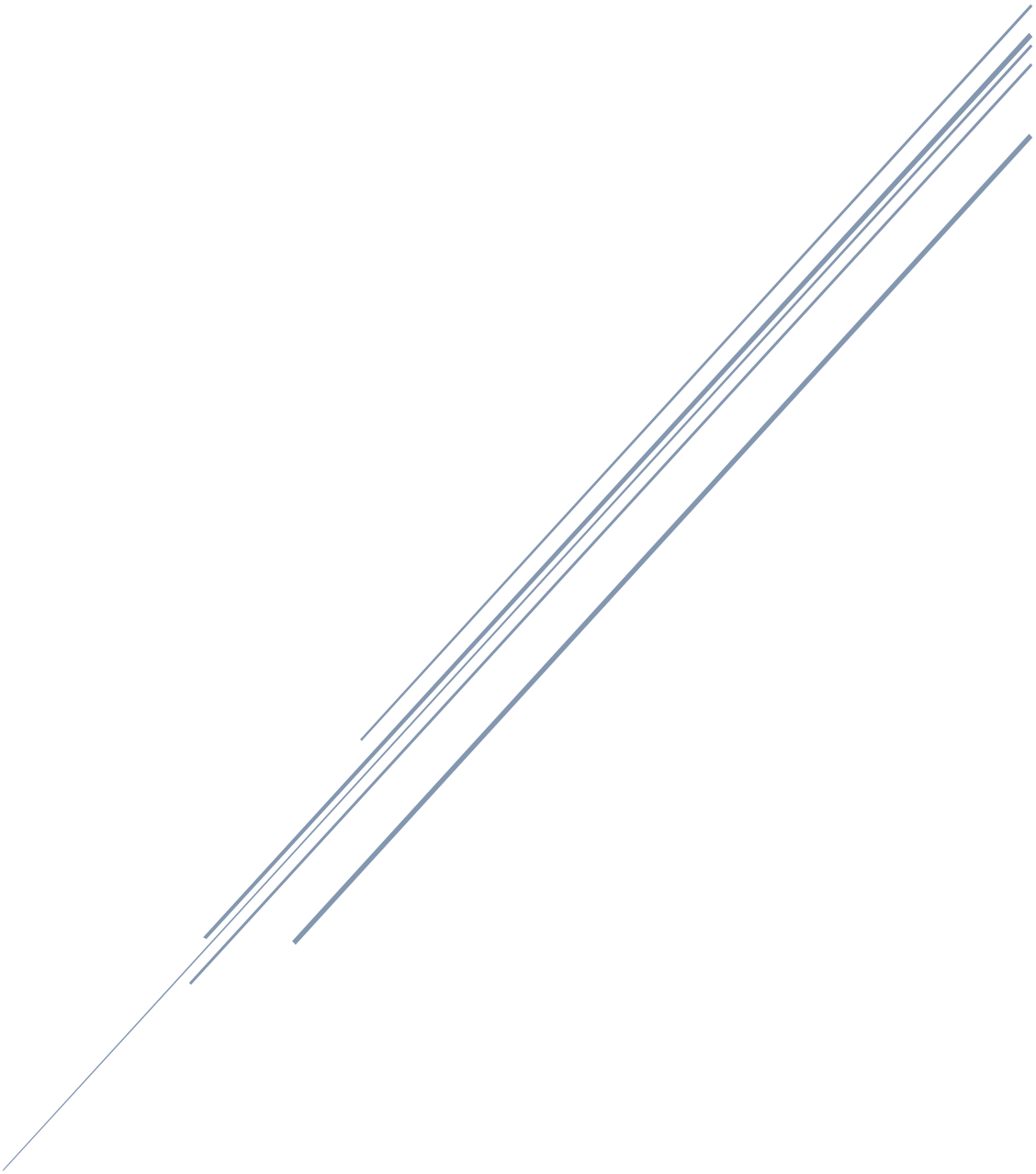

NMBU
Radioecology

A Preface

This master thesis commenced at the Norwegian University of Life Sciences (NMBU) within the faculty Environmental Science and Natural Resources Management (MINA). This thesis provides 60 ECTS and completes my master degree in chemistry with focus on Radioecology.

The practical work was completed at the Isotope Laboratory, by collaboration with the Center of excellence for Environmental Radioactivity (CERAD). This master thesis has enlightened my knowledge regarding release of radionuclides into the environment and the processes that occur in the aftermath. This knowledge has definitely added personal value to me.

I would like to thank my supervisor Hans-Christian Teien for introducing me to this thesis and for helpful guidance during the construction of methodology, Excel advices and constructive comments during the writing process.

I would also like to share my outermost gratitude to Marit Nandrup Pettersen, for laboratory training, instrument guidance, and the amount of time you invested in me during this thesis. Without your helping hand, I would have been lost.

Thank you to Brit Salbu and Ole Christian Lind for taking time to read my thesis and provide constructive corrections, and for your good advice. I would also like to thank Magne Simonsen for a helping hand and positive feedback during the writing. In addition, a general thanks to the rest of the staff and PhD students at the Isotope Laboratory. It was always very nice to enter the building.

It is also important for me to mention my employer, the Norwegian Coastal Administration, and my managers Jan-Ivar Meldre, Helge Munkås Andersen, Steinar Gyltnes and Kjetil Aasebø who allowed me to take time off work, even in busy times, to let me achieve this master thesis. A special thanks to Jan-Ivar Meldre for encouraging me to go ahead with this education. Also thanks to all of my brilliant colleagues at NCA, I missed you when I was at school.

At last, but not least I would like to thank my family. Thank you Clement for taking care of our girls and allowing me endless time to study. Thank you, Julie-Louise and Jenny-Linnea, for understanding the significance and giving me time off from your busy schedules. Without you, this would not have been achievable. Remaining family and friends: Thank you! For letting me off the hook when I was busy studying.

Birgitte Brockstedt Kvamme

Ås, 15th of May, 2019

B Abstract

In the event of a reactor accident, debris plumes containing artificially produced radionuclides could impose a great risk for the environment in distances far from the accident site. Radionuclides can enter the marine environment through atmospheric deposits and runoffs from terrestrial environment by rivers.

To evaluate the risk of radionuclides in marine systems, it is important to identify their physico-chemical form (speciation). The speciation of radionuclides are dynamic and changes in dissimilar water qualities e.g., in estuaries. Speciation of radionuclides will change by time and transport in coastal water. In water, cesium (Cs) can be present as different species, where the ions are more reactive and mobile than particles.

Utilizing numerical models as a tool to predict the atmospheric transport and deposition of radionuclides in the event of nuclear accidents can be helpful in risk assessments and in deciding where countermeasures are necessary. Such models are using the distribution coefficient, K_d, as a basis to estimate the water-sediment distributions. The K_d is the ratio between radionuclide concentrations in the particulate ($Bqkg^{-1}$) and in the dissolved phase (BqL^{-1}). K_d is site specific and depend upon the physico-chemical properties of both the radionuclide and the water-sediment system. If the system change, the K_d changes. Existing K_d values are based on the assumption that equilibrium conditions are valid, but such systems are, however, highly dynamic and more information about the dynamic changes are needed.

Recently, a numerical dispersion model was developed where speciation of Cs was included. To improve the dispersion model, more information about the changes of Cs species as a function of salinity and time are required. This master thesis provides such inputs to the dispersion model by generating experimental data of time dependent changes in Cs speciation by mixing freshwater with saline water and the use of gamma emitting ^{134}Cs and ^{137}Cs tracers to follow the processes. The experiments simulate the transformation processes in mixing zones that occur in the river outlet where fresh waters meet saline water. In the saline water, the ionic composition differs greatly from the riverine fresh water, leading to an alteration of the water chemistry, which again can change the radionuclide speciation, as well as components found in the river water, e.g. particles and humic substances.

Water and sediment samples were retrieved from the river Storelva situated in Risør, in south of Norway. The sorption of ^{134}Cs was studied by adding tracer to isolated riverine colloids and

clay. Further on, the riverine colloids and clay were studied as two compartment systems in brackish water designed to investigate;

(i) the remobilization of ^{134}Cs associated with riverine colloids and sorption of ^{137}Cs ions in saline water to riverine colloids as a function of increasing salinity and time

(ii) the remobilization of ^{134}Cs from clay and sorption of ^{137}Cs ions in saline water to clay as a function of salinity and time. The brackish water had an increasing salinity from 1 to 25 *PSU* (Practical salinity unit).

The compartment experiments lasted one month.

The Cs speciation was determined by utilizing size fractionation techniques at different timelines and the tracer activity was measured by a NaI-detector (PerkinElmer 2480 automatic gamma counter with wizard software).

The sorption of ^{134}Cs to riverine colloids had inconsistencies, compared to the sorption to clay. After 5 months only ±5 % ^{134}Cs was associated with the colloidal fraction while for the clay fraction, 99 % ^{134}Cs was associated with the clay fraction. This experiment is still ongoing.

The remobilization of ^{134}Cs from the riverine colloids was rapid in freshwater. As for ^{137}Cs accompanied by the saline water, there was only a minor association with the riverine colloids.

The remobilization of ^{134}Cs from riverine clay was minimum at the lowest salinities (1, 3 and 5 PSU) and then increased with salinity and time.

The ^{137}Cs sorption to riverine clay was higher for the low salinities. The ^{137}Cs was, mostly associated with the LMM fraction at high salinities.

The apparent K_d obtained in this experiment was in the range of 73-215 Lkg^{-1} for ^{134}Cs and 13-54 Lkg^{-1} for ^{137}Cs, decreasing with increasing salinity in line with literature data. The transfer rates, *k*, that describe the dynamic changes in transfer models, for both sorption and desorption were in the same magnitude in brackish water with low and high salinity. In general, the sorption rates (*k1*) seemed to decrease by salinity by a factor of 2, while the desorption rates (*k2*) were not dependent upon salinity.

C Sammendrag

Ved hendelser som involverer reaktor ulykker kan antropogene radionuklider, som transporteres til atmosfæren, utgjøre en stor risiko for det marine miljøet også på store avstander fra ulykkesstedet. Radionuklider kan tilføres det marine miljøet direkte ved atmosfæriske avsetninger og ved avrenning fra terrestrisk miljø til elver.

Radionuklider kan foreligge som ulike tilstandsformer i vann, som løste ioner, tilknyttet kolloider eller partikler. For å evaluere risikoen med radionuklider i marine systemer er det viktig å identifisere biotilgjengelighet og mobilitet til radionuklidene. Dette avhenger av tilstandsformen, hvor ioner er mere reaktive og mobile enn partikler. Fordelingen av de ulike tilstandsformene er avhengige av en rekke nøkkelfaktorer og ved endring av disse nøkkelfaktorene så vil tilstandsformene endres. Slike endringer finner sted for eksempel i estuarier der ulike vannkvaliteter blandes. Fordeling av tilstandsformer i estuarier vil endre seg som funksjon av tid og med økt innblanding av sjøvann.

Numeriske modeller er verktøy som blant annet kan benyttes for å simulere transport av radionuklider. Slike modeller benyttes for å vurdere risiko, for eksempel etter en atomulykke og for å vurdere hvor tiltak skal iverksettes. Slike modeller er basert på informasjon om hvordan radionuklidene vil fordele seg mellom vann og sedimenter, som uttrykkes ved fordelings koeffisienten K_d. K_d beskriver slik forholdet mellom partikulære og oppløste konsentrasjoner. Den vil variere fra sted til sted og er avhengig av de fysiske-kjemiske egenskapene til både radionukliden og vann-sediment systemet. Ved endring av de vannkjemiske forholdene vil også K_d endres. Eksisterende K_d verdier baserer seg på at det foreligger likevekt. Men naturlige akvatiske økosystem er høyst dynamiske og det er derfor behov for mer informasjon om dynamikken i endringene.

Nylig ble det utviklet en spredningsmodell hvor tilstandsformene til Cs ble inkludert. For å forbedre spredingsmodellene ytterligere er det behov for mer kunnskap om endringene i tilstandsformene til Cs som en funksjon av saltholdighet og tid. Målet med denne master oppgaven er å gi bidrag til utviklingen av spredningsmodeller, ved å generere eksperimentell informasjon om tidsavhengige endringer i fordeling av tilstandsformene til Cs i vann av varierende saltholdighet. Dette ble utført ved å bruke ^{134}Cs og ^{137}Cs tracer i ulike blandinger av ferskvann og sjøvann. Forsøket simulerte endringene som skjer i blandingssonene i elveutløp, der hvor ferskvann møter sjøvann. Det er spesielt den høye ione-konsentrasjonen i

sjøvannet og at sjøvann har høyere pH enn ferskvannet som påvirker tilstandsformene til Cs i en slik blanding.

Prøver av vann og sediment ble hentet fra Storelva som ligger i Risør, sør i Norge. Sorpsjon av ^{134}Cs ble studert ved å tilsette tracer til isolert kolloid- og leirefraksjon fra elven. Kolloid- og leirefraksjonen ble studert i to separate systemer i brakkvann utformet for å undersøke;

(i) remobilisering av ^{134}Cs assosiert med kolloidene og sorpsjon av ^{137}Cs-ioner i saltvann til kolloidene som funksjon av økende salinitet og tid.

(ii) (ii) remobilisering av ^{134}Cs fra leire og sorpsjon av ^{137}Cs-ioner i saltvannet til leire som funksjon av salinitet og tid. Brakkvannet hadde en økende saltholdighet fra 1 til 25 PSU (praktiske salinitetsenheter).

Mobiliseringsstudiene varte i en måned.

For å bestemme tilstandsformene til Cs ble det benyttet fraksjonering med hensyn på størrelse på fastsatte tidspunkt og tracer aktiviteten ble bestemt med en NaI-detektor (PerkinElmer 2480 automatic gamma counter with wizard software).

Det var stor forskjell i sorpsjon av ^{134}Cs til kolloider og til leire i elvevannet. Etter 5 måneder var kun ±5% assosiert med den kolloidale fraksjonen mens for leire var hele 99% ^{134}Cs assosiert med leire. Dette sorpsjonseksperimentet pågår fremdeles.

Remobilisering av ^{134}Cs fra kolloidene var hurtig i ferskvann og sorpsjon av ^{137}Cs fra saltvannet til kolloidene var minimal.

Remobiliseringen av ^{134}Cs fra leire var minimal ved de laveste saltholdighetene (1, 3 og 5 PSU) og økte deretter med økt saltholdighet og tid.

Det var høyere sorpsjon av ^{137}Cs fra saltvann til leire i brakkvann med lav saltholdighet. For brakkvann med høyere saltholdighet var ^{137}Cs for det meste assosiert med LMM fraksjonen.

Den tilsynelatende K_d var i området 73 - 215 Lkg^{-1} for ^{134}Cs og 13 - 54 Lkg^{-1} for ^{137}Cs og avtok som en funksjon av økende saltkonsentrasjon på lik linje som i litterære data.

Endringskoeffisientene, *k*, som forklarer de dynamiske endringene for både sorpsjons og desorpsjons var i samme størrelsesområde for brakkvann med lav og moderat saltholdighet. Generelt, avtok sorpsjonsratene (*k1*), grunnet saltholdighet med en faktor på 2, mens desorpsjonsratene (*k2*) viste ingen endringer grunnet saltholdighet.

Index

1 Introduction

Radionuclides can enter the marine environment through atmospheric deposits and runoffs from terrestrial environment by rivers. In the event of a reactor accident, debris plumes containing artificially produced radionuclides could impose a great risk for the environment in distances far from the accident site. This was demonstrated by fallout from the Chernobyl accident in 1986. The accident resulted in deposition of large fuel particles, with variable radionuclide composition, within a 30 km zone with respect to the plant, while small-sized particles were identified up to 2000 km from the site (Devell et al., 1968; Salbu, 2000). The Chernobyl accident resulted in large deposits of radiocesium in central Norway, especially in mountainous areas like Valdres and Jotunheiemen (Baranwal et al., 2011; Skuterud et al., 2014). Other sources to artificially produced radionuclides transport to the marine environment are global fallout from nuclear weapons testing and discharges from radioactive waste and nuclear facilities like Cap de Haag in France or Sellafield and Dounreay in the UK (UNSCEAR, 2000).

In water, cesium (Cs) can be present in different physico-chemical forms having different properties, where the ions are more reactive and mobile than particles. The transfer of radionuclides are such highly dependent upon speciation where the radionuclide ions are most bioavailable (Salbu, 2004). Information regarding speciation is essential for risk assessments (Salbu, 2016). To evaluate the risk of radionuclides in marine systems, it is important to identify the size distribution of radionuclides. The speciation of radionuclides are, however, dynamic and changes with changing water qualities e.g., in estuaries where freshwater rivers enters salt water. Speciation of radionuclides will change by time and transport in coastal water.

The distribution coefficient, K_d, is site specific and depends on the physico-chemical properties of both the radionuclide and the water-sediment system. If the system change, the K_d is affected (P. Ciffroy et al., 2001). The changes can be related to the speciation of the radionuclide or an alteration in the water-sediment chemistry, such as salinity alterations in an estuary.

Numerical models exist to predict the transportation and fate of radionuclides in the marine environment (e.g., Perianez et al., 2016a; Simonsen et al., 2017; Vives i Batlle et al., 2018). Utilizing models, as a tool to predict the atmospheric transport and deposition of radionuclides in the event of nuclear accidents, can be helpful in deciding where countermeasures could be needed. Therefore, generic and operationally available preparedness models for marine radionuclide contamination are necessary for fast-response in emergencies (e.g., Duffa et al.,

2016). Such models are using distribution coefficients (K_d) as a basis to estimate the water-sediment distributions. Existing K_d values assume that equilibrium conditions are valid, but such system is, however, highly dynamic and more information about the dynamic changes are needed. When non-equilibrium conditions exist, the apparent K_d can be used (Strandring et. al., 2002).

In previous models the speciation of the radionuclides have often been ignored (e.g., Karcher et al., 2004; Orre et al., 2010; Tsumune et al., 2013; Simonsen et al., 2017). As the speciation of radionuclides are important to assess the overall environmental consequence of an accidental release, this has become more common to include in models (Aldridge et al., 2003; Smith et al., 2003; Kobayashi et al., 2007; Choi et al., 2013). However, to incorporate the speciation into models still has some gaps in knowledge, as these processes are not yet fully understood (Salbu, 2016). Recently, a transfer model was developed, where speciation of Cs was included (Simonsen et. al., 2019). The study was based on a hypothetical accidental release of Cs from HAL - storage tanks (High Activity Liquor) at Sellafield in UK during a storm as the main contributor to the model. The scenario included deposited Cs on land, and subsequent run-off by rivers to the marine environment.

Simonsen has also developed a transport model of trace metal species in the Sandnesfjord (Simonsen et. al, 2019). The model incorporated element speciation, based on measured distribution of aluminum speciation as a function of time and distance from the outlet of the freshwater river Storelva into the Sandnesfjord.

In general, the transport model was able to reproduce the distribution of trace metal concentration and speciation in coastal waters. However, the study showed that the model had improved if background levels of trace metals, originating from the coastal water, were included, as this lead to an underestimation of the trace metal concentration. The model also overestimated the near-surface vertical mixing, resulting in an under estimation of the trace metal in surface waters. In addition, the model showed a good correlation between the measured and estimated distribution of trace metal species during low-flux periods. While a weaker correlation between the predicted surface salinity and total trace metal concentration during high-flux periods were recognized. The study proved that by including the changes in metal speciation (transfer rates), the prediction of the distribution of total contaminant and concentration levels of element species where improved.

At current time, there is few such data available for Cs and more information is highly needed about the changes of Cs speciation as a function of salinity and time to improve the transfer models. This master thesis provides such inputs to the dispersion model by generating experimental data of time dependent changes in Cs speciation by mixing freshwater with saline water and the use of gamma emitting ^{134}Cs and ^{137}Cs tracers to follow the processes. Both the remobilization of Cs from colloidal and particulate material transported by the river as well as the sorption of Cs in marine environment was investigated. The experiments simulated the transformation processes in mixing zones that occur in the river outlet where fresh waters encounter saline water. The Cs speciation information was obtained by utilizing size fractionation techniques at different timelines.

1.1 Goal for master thesis

The overall goal for this master thesis is to establish information on the transfer of Cs species in fresh waters to coastal areas. Hence, the work will focus on the dynamic water-sediment distribution coefficients and transfer-rates of Cs species as a function of salinity and time.

The hypotheses is:

H0: The distribution coefficient (K_d) of Cs between radioactivity in water and sediment is dynamic and dependent on salinity and will vary in brackish water with increasing salinity.

H1: Remobilization of Cs from riverine colloids and particles is more prominent for the marine transport than sorption of Cs to surfaces in saline waters.

2 Background

2.1 Estuaries

Estuaries, defined as a semi-enclosed coastal body and a mixing zone, have connection to the open sea. In estuaries, saline water dilutes with fresh water due to run-off from land drainage (Pritchard, D.W., 1967). In general, estuaries have a regular variation of low to high salinity concentrations when moving from river-outlet to the open sea. The variations in salinity is both horizontal and vertical, where the salinity occasionally increases by depth as an effect of higher density of saline water. Seasonal changes due to ice melting, floods, wet and dry periods e.g. will affect the arrangement in the estuary (vanLoon G.W. & Duffy S.J., 2011). In estuaries, the concentration of several trace metals and radionuclides decrease due to an increase in salinity and by dilution through saline water with lower concentrations of trace metals (Simonsen et. al., 2017).

2.2 Properties of cesium

In nature, Cs is present as the stable ^{133}Cs isotope. In addition, Cs exist as ^{134}Cs and ^{137}Cs radioactive isotopes. ^{134}Cs and ^{137}Cs, both gamma emitters, are fission products from nuclear power plants and have a half-life of 2 and 30 years respectively (Dietz et. al., 1963). Cs can be present as large entities like fragments or particles (>0.45 µm) or as simple Cs-ions. The Chernobyl accident resulted in large deposits of both ^{134}Cs and ^{137}Cs across Europe (OECD, 1996; CEC, 1998).

Cesium is very soluble and the mobility of both ^{134}Cs and ^{137}Cs in marine environments are highly dependent on contact time between the radionuclide and the sediments (Børrentzen P., Salbu B. 2002; e.g. Oughton, Børretzen, Salbu & Tronstad, 1997). The fate of Cs in freshwater and the marine environment depend on the physico-chemical properties of the radionuclide and the physical, chemical and biological composition of the water. The physico-chemical properties of radionuclides are their molecular mass, interacting ligands, crystallographic structure, oxidation state, charge properties and magnetic properties. The composition of water like the salinity, the content of complexing organic and inorganic ligands like carbonates, the pH and the redox state will influent the speciation of the radionuclide (Salbu 2000b; Salbu et al., 2004b).

The physico-chemical speciation of Cs is dependent on many influencing factors in fresh water, as well as in coastal and marine water. Trace metals and radionuclides can be present

as, either, particles, high molecular masses like colloids or low molecular masses (LMM) like simple ions (Salbu, 2009). Due to their size (>0.45μm) and high density, particles will most likely undergo sedimentation in the water phase. Particles will not easily bioaccumulate in organisms. However, particles can be retained in bottom dwelling and filter feeding organisms like mussels, and bioaccumulate (Jaeschke *et* al., 2015; Børretzen and Salbu, 2009). Particles associated with sediments can remobilize due to weathering, hence become bioavailable and induce ecosystem transfer by time (Kashparov *et* al., 1999). Colloids are smaller (<0.45 μm – 10 kDa), due to this colloids will not settle and are kept in solution. The low molecular masses (LMM) are small (<10 kDa), mobile, bioavailable and easily taken up in organisms. LMM is the speciation of most concern, as they will bioaccumulate in biota and can interfere with normal homeostasis within the cells of an organism (Teien *et* al., 2006). Especially the reactive LMM species absorbs in specific tissues and target organs through external body exposure or through contaminated food or water (Carvalho, 2018).

Estuaries where freshwater enter coastal water are in non-equilibrium conditions and are dynamic systems, meaning they will change over time (Periáñez et al., 2018). Thus, in coastal water, the speciation of radionuclides such as Cs will change by time. LMM can aggregate and turn into colloids, or radionuclides associated with colloids or particles can remobilize to LMM species due to the presence of competing ions in saline water. In general, the remobilization of radionuclides associated with riverine particles or colloids increase in line with the salinity. This may lead to a higher concentration in LMM species locally, even though there is a high degree of dilution in estuaries (Teien et al., 2006; Machado et al., 2016; Sanial et al., 2017). In such mixing zones the speciation is highly dependent on the properties of the recipient water (pH, humic content, presence of competing ions, salinity, currents, water flow (river) and waves (ocean) e.g.) (Salbu, 2000b).

2.3 Size and charge fractionation techniques

Size and charge fractionation techniques can distinguish between radionuclide species in water. These techniques are applicable for trace metals as well. Using size and charge fractionations techniques in water, before determination of the radionuclides in collected fractions, can provide information about the speciation of radionuclides present in water and their physico-chemical properties (Salbu, 1985).

2.4 Binding of Cs to clay and colloids

The characteristics of sediments influence the degree of Cs-binding. In the contraire to sand and silt, clay is highly reactive due to a large surface area (Rose, 2005). Clay minerals offers many binding sites for Cs and the degree of binding are dependent on factors like the presence of competing ions (K^+, Na^+, Ca^{2+}) and the sorption time. Radiocesium can a) sorb to the clay surface and planar sites and is easily exchangeable with other ions in general, b) sorb to wedge sites and is exchangeable with cations of similar size and charge, or c) sorb to interlayer clay sites where cesium is not readily exchanged, hence, regarded as fixed (Evans, Alberts Clark III, 1983). According to Børretzen, P. and Salbu, B. (2002) the planar sites on the clay surfaces are considered "reversible binding sites", the wedge sites on the clay mineral are considered as "slowly reversible binding sites" and the interlayer sites on the clay mineral are considered as irreversible binding sites (figure 1) (Børrentzen P., Salbu B. 2002).

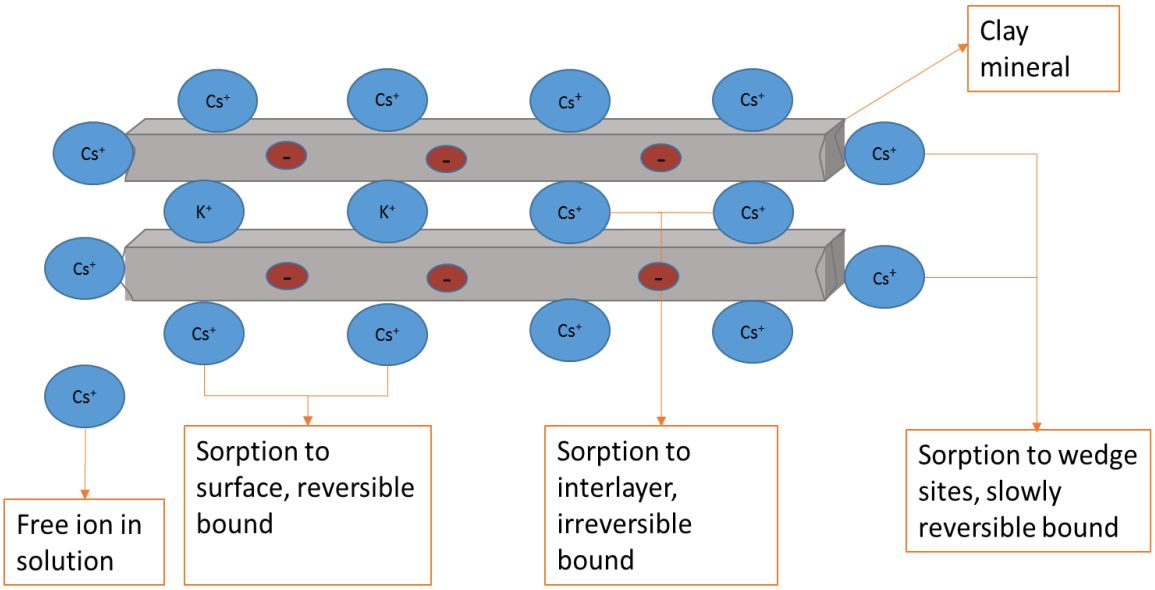

FIGURE 1 CESIUM SORPTION TO CLAY MINERAL BY SORPTION TO WEDGE SITES, SORPTION TO SURFACE AND SORPTION TO INTERLAYER. THE DEGREE OF BINDING DEPENDS ON TIME, COMPETING IONS, PH, SALINITY. FIGURE REPRINT FROM BØRRENTZEN AND SALBU 2002.

Clay minerals can be present in the water phase due to erosion (storm, flood e.g.) or in the sediment bed. When riverine clay minerals, contaminated with radiocesium, transports to the ocean, the changes in salinity will affect the binding sites and Cs can remobilize to the water phase. Since ion exchange is prevailing on the clay mineral (Cornell, R. 1993), competing ions in saline water will exchange sites with Cs.

Dissolved organic matter, like humic material (HM) or colloids, in freshwater systems origins primarily from plant or microbial residues. Colloids suspended in lakes or rivers will not aggregate, due to repelling forces of the similar net charge on the colloid, resulting in long lasting suspension of colloids (vanLoon G. W. & Duffy J. D., 2011). However, in the presence of ions with suitable charge, ions will undergo sorption to the colloids, providing with an overall net zero charge; hence, colloids act as transporting agents in natural water systems (Kersting et al., 1999; Salbu, 2000; Novikov et al., 2006). In estuaries, where riverine colloids enters high saline water, they aggregate due to the high levels of the competing ion, Na+, hence increasing their size and density. Due to this and the general decrease of the river water flow, observation of sedimented colloids in estuaries are common (vanLoon G. W. & Duffy J. D., 2011). Cs adsorbs to colloids through ionic and covalent bonds (Figure 2).

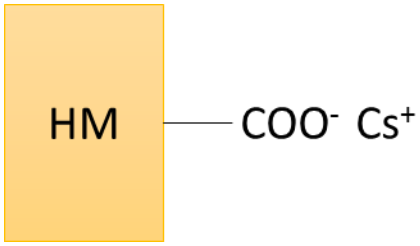

FIGURE 2 CS BONDED TO HUMIC MATERIAL (HM) BY ELECTROSTATIC FORCES (VANLOON G.W. & DUFFY J. D., 2011).

The strength of the interaction between metals and humic material depends on the properties of the metal, number of binding sites on the colloid and HM functional groups available for complexing reactions, pH and the presence of other competing ions. In estuaries, where high levels of competing ions are present, since Cs is monovalent ions they are generally desorbed, especially in the presence of Al^{3+} ions, which is a trivalent ion whom tend to be strongly bonded to humic material (vanLoon G. W. & Duffy J. D., 2011).

2.5 Transfer rate

To interpret the speciation in dispersion models, Simonsen developed new equations where the dynamic changes in the system are included (Simonsen et. al. 2019). The equations builds on the theory that a specie transfers into another specie during a time step, referred to as dynamic transfer rates (e.g., Periáñez, 2005). High transfer rates indicate rapid transfer processes, and low transfer rates indicate a slower specie transformation.

The transfer rate is the quantity of the concentration transferred to another specie in a given time. Figure 3 illustrates the transformation processes between ions and particles, assuming only reversible sorption. Where desorption, are also referred to as remobilization.

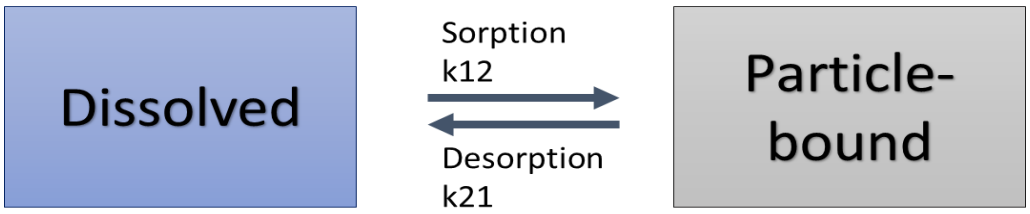

FIGURE 3 A SIMPLIFIED SYSTEM INVOLVING THE DISSOLVED AND THE PARTICLE-BOUND SPECIES ILLUSTRATING THE TRANSFORMATION PROCESSES (FIGURE REPRINTED FROM PERIÁÑEZ, 2012)

The transfer rates are calculated by equation 1 and 2. Equation 1 and 2 assumes reversible processes and incorporates the dynamic changes in the system. This gives one equation for the dissolved species (LMM (C_w), and one for the particle-bound species (C_p).

$$\frac{\partial C_W}{\partial t} = adv_w + diff_w - k_{12}C_w + k_{12}mC_p \quad (1)$$

$$\frac{\partial (mC_p)}{\partial t} = adv_p + diff_p + k_{12}C_w - k_{21}mC_p \quad (2)$$

K_{12} and k_{21} are the transfer rates for sorption and desorption respectively, m is the mass density of suspended particulate mass (SPM) in the water column and $adv_{w,p}$ and $diff_{w,p}$ are the convergence of advective and diffusive terms for the dissolved and the particle bound fractions. In a closed system the $adv_{w,p}$ and $diff_{w,p}$ will be zero.

Transfer rates utilized in previous models on the distribution of Al-species in the estuaries in Sandnesfjord (Simonsen et. al., 2018) for both sorption (*k12)* and desorption (*k21)* were in the range of $1x10^{-4}$ s^{-1} to $1x10^{-5}$ s^{-1} where sorption rates decreased with an increasing salinity and desorption rates increased with increasing salinity. However, these are transfer rates for aluminum with other element properties than Cs and a direct comparison should emphasis

carefulness. Nonetheless, the changes in the transfer rates due to salinity are eligible for comparing.

Periáñez (2012) has also calculated sorption rates for Cs, these rates were in the range $1.0x10^{-5}\ s^{-1}$.

2.6 Distribution coefficient, K_d

In the marine environment, radionuclides are distributed between the dissolved phase and the particulate phase, the fate and bioavailability strongly depends on this distribution and on the strength of the radionuclide association (P. Ciffroy et al., 2001). The distribution is characterized by the distribution coefficient (K_d). The K_d is the ratio between the particulate and the dissolved concentration and is time dependent.

If radionuclides are released to freshwater or saline water from the soil or sediment, the theoretical mobility will depend on the K_d (Equation 3).

$$K_d = \frac{concentration\ of\ radionuclide\ in\ soil/sediment}{concentration\ of\ radionuclide\ in\ water} \qquad (3)$$

Analysis of contaminated surface sediments and water collected in the field or kinetic model experiments using tracers can provide information about the K_d (Skipperud et al., 2000a; Skipperud et al., 2000b; Salbu, 2000b). The K_d is unique for each radionuclide and will vary according to the salinity, pH and temperature in the water and likewise the components in the soil and sediment. The K_d is highly site specific, and will vary in different locations.

Low K_d values indicate that the element of interest is mobile, conservative or non-reactive, whereas high K_d values indicates that the element is particle-reactive or non-conservative. IAEA (2004) recommend K_d values, however the uncertainties regarding these K_d values should not be neglected. K_d is obtained when a state of equilibrium is achieved (IAEA 2004). The state of equilibrium is hard to obtain in the environment, as systems are in constant changes due to natural weathering processes. Therefore, in practice, such conditions are hardly ever obtained, and the equilibrium distribution is not very useful in model applications (Periáñez et al., 2018). The apparent K_d, defined as a distribution coefficient under non-equilibrium conditions can

provide information about an expected area where the distribution coefficient would reach equilibrium at a given time and salinity (Strandring et. al., 2002).

Based on reported K_d values, Cs is considered particle reactive (K_d = 2.9 x10^4Lkg^{-1} (IAEA, 2010)) in freshwater, meaning that Cs will interact with other components in the water phase. In saline water, Cs is considered less particle reactive as the K_d is lower (K_d = 2 x10^3 Lkg^{-1} (IAEA, 2004)). When Cs enters the ocean, particle reactivity decrease as a direct result of the presence of competing ions.

3 Materials and Method

This method covers the remobilization of Cs from riverine colloids and clay studied in a controlled laboratory experiment. The colloids and clay were added water of different salinity (brackish water), thus simulating river outlet into brackish water. In addition, sorption of Cs from saline water to colloids and clay in the brackish water were studied. The remobilization and sorption experiments were performed using ^{134}Cs and ^{137}Cs as tracers simultaneously.

The riverine colloids and clay were studied as two separate compartment systems in brackish water. Two compartment systems were established designed to investigate;

(i) the remobilization of ^{134}Cs associated with riverine colloids and sorption of ^{137}Cs ions in saline water to riverine colloids as a function of increasing salinity and time

(ii) the remobilization of ^{134}Cs from clay and sorption of ^{137}Cs ions in saline water to clay as a function of salinity and time. The brackish water had an increasing salinity from 1 to 25 *PSU* (Practical salinity unit).

The remobilization experiment lasted one month, whereas the sorption experiment had a one-year timeline. The latter is still an ongoing experiment.

3.1 Sources

The sampling area chosen for this master thesis was the River Storelva situated in Risør, Aust-Agder in south of Norway. Storelva is part of the Vegårvassdraget and runs out into the Sandnesfjord. The Storelva is approximately 13 kilometers long. Due to acidification, Storelva has been limed since 1983, the river still has some variables in pH (Norwegian Environmental Agency, 2016). Figure 4 shows a map of the area and the sampling site.

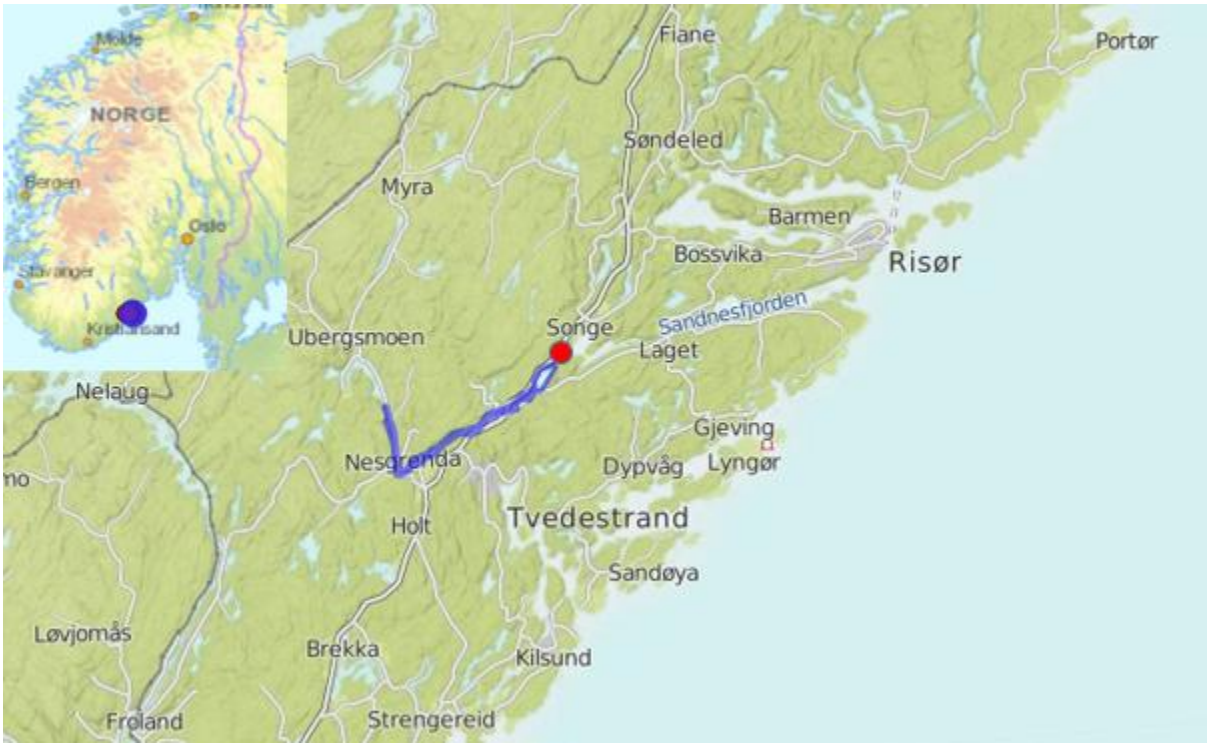

FIGURE 4 STORELVA RUNS OUT INTO SANDNESFJORD. STORELVA IS MARKED WITH BLUE LINE AND THE SAMPLING SITE FOR WATER AND SEDIMENTS MARKED WITH RED.

Sediment and water samples were collected upstream the outlet of the river Storelva in November 2018. The river water was sampled filling 25 L containers directly from the river. A grab was used to retrieve the sediments. Several grabs of sediments from the same site were transferred to a 5 L bucket. Both water and sediments were stored dark at 4 °C prior to use.

By retrieving sediments and riverine water from Storelva, the hypothesis could be tested. By adding the tracer ^{134}Cs to the riverine sediments and applying brackish water with different salinities, the speciation of the tracer would most likely change. The ^{137}Cs tracer added to the saline water illustrated the sorption of Cs ions from the saline water to riverine sediments. Utilizing size fractionations, the speciation of the tracers were followed over time. Information regarding the distribution of the tracers provided information about K_d given at different salinities as well as sorption rates.

3.2 Isolation and concentration of colloids

A 0.45µm High Capacity In-Line Groundwater Sampling Capsule excluded particles from the Storelva riverine water before further processing (Figure 5). The colloidal fraction present in riverine water was prepared by recycling the water through a 10 *kDa* hollow-fiber hence removing the LMM fraction. Using this method reduced 8L riverine water to 800 mL colloidal suspension. Standard curve for determination of Total Organic Concentration (TOC) was made based on samples measured in a TOC analyzer (TOC-V cpn, Shimadzu), and the concentrated colloidal fractions were measured photometric (UV-1800 spectrometer, Shimadzu) towards this curve.

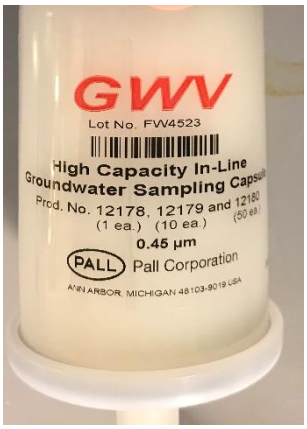

FIGURE 5 0,45 µM FIBER USED FOR EXCLUDING PARTICLES.

3.3 Isolation and concentration of clay

Clay fraction from the Storelva sediments were isolated at the Isotope lab at Ås using a modified in-house method developed by A.O. Stuanes (NLH, 1998). Figure 6 illustrates the steps in this procedure.

First, a 2 mm sieve removed the gravel and plant debris, leaving the sand, silt and clay fraction. Second, a 0.63 mm sieve removed the sand fraction. Sedimentation due to Stokes law removed the silt fraction. The water-clay suspension was transferred to a bottle before the clay suspension was concentrated by flow through a 10 *kDa* hollow-fiber. 2 L of the clay suspension was concentrated down to 800 ml by removal of the water in LMM-fraction.

To determine the mg clay present in the clay suspension 3 parallels of each 1 ml was pipetted and dried at 60°C in approx. 2 h, and then the weight was determined by an analytical balance with an accuracy of 0.001 g. This gave the mg clay / ml clay-suspension. Appendix E contains the experimental weights.

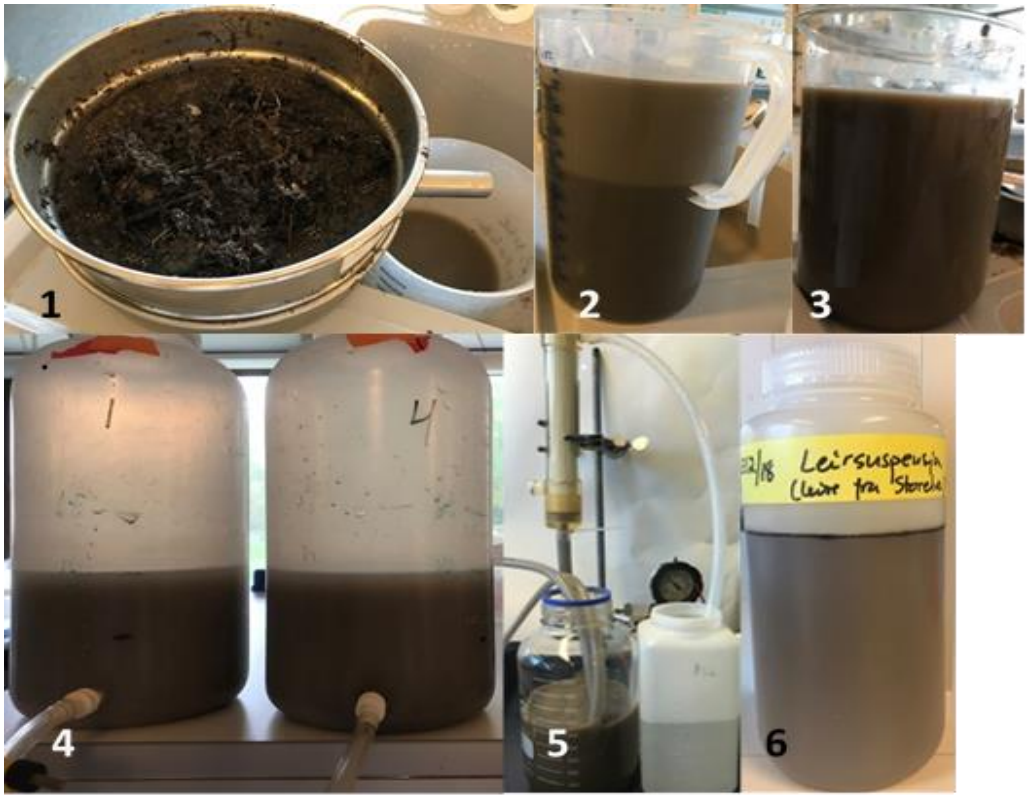

FIGURE 6 THE ISOLATION OF CLAY FROM THE SEDIMENTS. (1) SIEVES ISOLATES THE CLAY AND SILT FRACTION (2 AND 3), SEDIMENTATION BY STOKES LAW (4) AND FLOW THROUGH HOLLOW-FIBER WITH REMOVAL OF THE LMM FRACTION (5) TO CONCENTRATE THE CLAY SUSPENSION (6).

3.4 Preparation of experimental water

3.4.1 Riverine water from Storelva

Conductivity and pH were measured. The pH meter (WTW Multi 340i with pH electrode Sentix 41) was calibrated daily using buffers at pH 4.01 and pH 7.00. Conductivity was determined by means of the WTW Multi340i with a TetraCon electrode. The major cation and stable Cs concentrations were determined using ICP-MS (Agilent 8900, Japan).

3.4.2 Artificial riverine water

Using artificial river water in the experiment ensured low levels of TOC. The ionic composition, pH and conductivity of riverine Storelva water was analyzed using ICP-MS. Artificial riverine water mimicked the ion composition and concentration of the riverine Storelva water. A stock ion solution (100 times concentration of Storelva) was diluted using Type II purified water, and was then measured for pH and conductivity to achieve the same as the Storelva riverine water.

The artificial riverine water was the washing agent for the marked clay and colloidal suspension, and a component to make the brackish water.

3.4.3 Saline water

Saline water retrieved from NIVA MF Solbergstranda in the Oslofjord (experimental collected at 40 m depth), had a salinity at 31.9 *PSU* (Practical Salinity Unit). A 0.45µm filter and a 10 *kDa* hollow-fiber removed particles and HMM organic matter in the saline water. This left the LMM fraction in the saline water for experimental use and ensured minor influence from organic matter within the experiment. The saline water contributed to making the gradient brackish water in the experiment.

3.5 Sorption of Cs tracer to riverine colloidal and Clay fraction

The use of radioactive tracers gained information about the distribution of species in the system. Whereas, ^{134}Cs and ^{137}Cs tracers were added to the clay and colloidal (HMM) suspension and the saline water, respectively.

Before using radioactivity in experiments, a BAT (Best Available Technique) and a RAV (Risk and Vulnerability Analysis) were performed to justify the use of radioactivity, and to ensure good laboratory practice and waste control.

The ^{134}Cs tracer was added the riverine colloidal and clay fractions according to table 1. The Cs tracers were added as Cs-ions from a weak acid tracer solution.

Table 1: Overview of total amount of suspensions and the nominal activity added each suspension.

Suspension	Total volume of suspension (mL)	Activity of ^{134}Cs (*Bq*)
Colloidal	800	18100
Clay	800	18100

Roller tables kept the particulate matters in suspension. Experiments were conducted in room temperature (~20°C).

To follow the changes in the size distribution of ^{134}Cs, suspensions were fractionated with respect to size. To obtain this information, 0.45 µm syringe membrane filters (VWR 0.45 Polyetersulfone (PES) membrane, prod. no. 514-0075) and 10 *kDa* ultrafiltration membrane

filters (Amicon Ultra-15 10K Centrifugal Filter Devices operating at 4000 rpm in 15 minutes) were used according to Salbu.et al., 1985. Fractionations were performed at time intervals, 1 hour, 1 day, 1 week, one and 5 months. The NaI-detector (PerkinElmer 2480 automatic gamma counter with wizard software) determined the activity in each fraction (LMM, colloidal, >0.45µm).

3.6 Mixing of riverine colloids with brackish water

An aliquot of the riverine colloid suspension marked with ^{134}Cs was extracted. The contact time between the riverine colloids and the tracer was 5 days before separation. The activity concentration of ^{134}Cs associated with the LMM fraction in the riverine colloidal suspension was excluded by using artificial river water as a washing agent. The riverine colloidal suspension was diluted and then filtered through a 10 *kDa* hollow-fiber (SLP 0053, PALL) until the original volume and TOC was achieved (measured spectrophotometric) (figure 7).

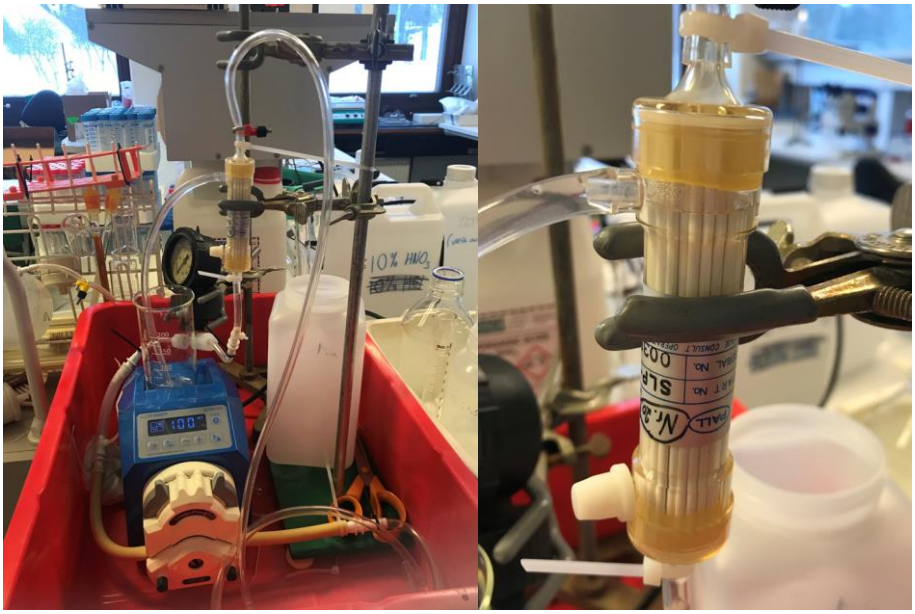

FIGURE 7 SHOWS THE HOLLOW-FIBER FILTRATION UNIT WITH MESH SIZE 10 *KDA* EITHER ISOLATING OR REMOVING THE LOW MOLECULAR MASSES. A PERISTALTIC PUMP PROVIDES VACUUM IN THE SYSTEM.

The washing procedure was repeated three times, assuming removal (dilution) of the LMM marked fraction. The wastewater was measured on the NaI-detector.

Samples were prepared in centrifugal tubes (50mL) according to table 2 with three replicates.

Table 2: The mixture ratio of different waters used to prepare the brackish test waters of different salinities (*PSU*).

Practical Salinity Unit (*PSU*)	mL saline water (*100 Bq* ^{137}Cs)	mL colloidal suspension (marked with ^{134}Cs)	mL artificial river water
1	1.6	10.8	37.6
3	4.7	10.8	34.5
5	7.8	10.8	31.4
10	15.7	10.8	23.5
15	23.5	10.8	15.7
25	39.2	10.8	0

To ensure equal activity and relatively stable speciation of ^{137}Cs in each replicate, the saline water from table 2 was added 100 μl ^{137}Cs tracer solution (^{137}Cs activity: 1032 *Bq*/ml) one day prior to additional sample preparation. This also allowed some contact time between the saline water and the tracer. To ensure the tracer was present as Cs-ions, marked saline water was centrifuged by a 10 *kDa* ultrafiltration membrane (Amicon Ultra-15 10K Centrifugal Filter Devices operating at 4000 rpm in 15 minutes) before use and activity in the filtrates analyzed by the NaI-detector.

Before adding the colloidal suspension to the centrifuge tubes, artificial river water diluted the marked ^{137}Cs saline water. This to avoid remobilization of ^{134}Cs due to high salinity. Roller tables kept the samples in suspension. Experiment executed at room temperature (~20°C).

To follow the changes in the system and the distribution of ^{134}Cs and ^{137}Cs species after introducing the brackish saline water, sampling (~8mL) by syringe was performed after 0.5h, 2h, 5h, 24h, 8 and 30 days of interaction.

To obtain information on the distribution of Cs-species, fractionation by 0.45 µm syringe membrane filter (VWR 0.45 PES membrane) and 10 *kDa* ultrafiltration membrane (Amicon Ultra-15 10K Centrifugal Filter Devices operating at 4000 rpm in 15 minutes, swing-out rotor) was performed (Figure 8).

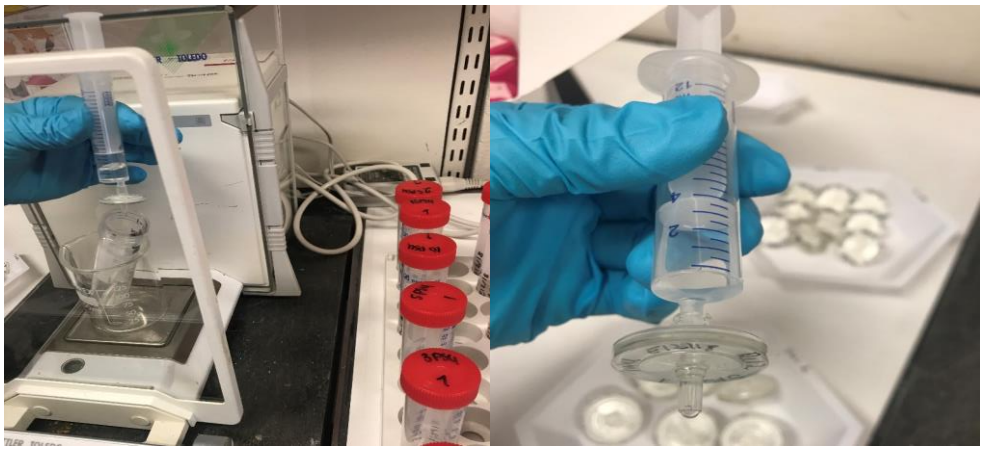

FIGURE 8 SAMPLES FILTERED BY 0.45µM SYRINGE MEMBRANE FILTER AND 10 *KDA* ULTRAFILTRATION MEMBRANE.

Thus, size fractionation techniques separated and determined in which size range the ^{134}Cs and ^{137}Cs species were:

- Particle (clay) (>0.45μm)
- High molecular mass (HMM) / colloidal fraction (>10 kDa ≤0.45 μm)
- Low molecular mass (LMM) (≤10 kDa)

An analytical balance with an accuracy of 0.001g determined the weights. Appendix B contains the experimental weights. The activity concentration of ^{134}Cs and ^{137}Cs in each fraction was determined by using a NaI-detector (PerkinElmer 2480 automatic gamma counter with wizard software) (Appendix D).

3.7 Mixing of riverine clay with brackish water

The same method as for the riverine colloids applied when determining the system changes in the riverine clay suspension. Allowing the clay suspension 6 days of contact time with the ^{134}Cs tracer prior to mixing with brackish saline water. To avoid sedimentation of the clay in suspension, clay samples were constantly in movement by roller tables or magnetic stirrers when preparing aliquots and extracting samples. Appendix A - D contains the analytical weights and the measurements with the NaI-detector.

3.8 Determination of stable Cs and radiocesium

The activity in samples was counted by using the NaI-detector (PerkinElmer 2480 automatic gamma counter with wizard software). The NaI-detector has an auto sampler, which allows

running a large quantity of samples. Three replicates were analyzed and counting time for each sample was 15 minutes. Analytical blanks determined the background radiation. Standards was used to ensure low counting errors (^{137}Cs test tube check source, PerkinElmer, IAEA 300/IAEA 373 reference materials). In addition, "house" standards of ^{134}Cs and ^{137}Cs as separate and mixed solutions was prepared to ensure good specter overlap control and to determine the counting efficiency within the energy spectra. The wizard software was set up to count both ^{134}Cs and ^{137}Cs sample at the same time.

To quantify the concentration of stable Cs (^{133}Cs) in the experimental waters, ICP-MS (Agilent 8900)) was utilized.

3.9 Data handling

3.9.1 Calculation of activity obtained by the NaI detector

The activity obtained by the NaI detector was adjusted according to background radiation from analytical blanks and the counting efficiency of the instrument (Equation 4). This gives the *dpm*, disintegration per minute.

$$DPM = \frac{CPM_{sample} - CPM_{blank}}{Efficiency} \qquad (4)$$

Cpm (counts per minutes) is the detected signals from the sample due to radioactive decay, and *dpm* is the given activity in a known reference material. Activity of the reference materials are given in Becquerel, Bq, defined as disintegrations per second (Choppin, G., Liljenzin, J. O. & Rydberg, J., 2016). By rearranging equation 4, the efficiency of the instrument was obtained.

The quantification limit was calculated based on 10 times the standard deviation of *cpm* from 10 blank samples. If the *cpm* sample was lower than the quantification limit, then the activity could not be quantified in the sample.

K_d was calculated by dividing *dpm pr. kg.* of particle (dry weight) divided by *dpm pr. L* water.

The transfer raters, of sorption (*K12)* and desorption *(K21)* illustrated in figure 3, was calculated by Simonsen M. and Saetra Ø (Appendix G).

3.9.2 Data analysis

The *dpm* was calculated for all replicates (LMM fraction, colloidal fraction and >0.45μm fraction) and organized in excel. The percentage distribution was calculated and the average of 3 replicates were graphically plotted pr. time or pr. salinity including the standard deviation for each sample replicate (3 replicates for each salinity).

4 Results and discussion

4.1 Traceability and precision

The uncertainty and precision of the NaI-detector depends on the counting time and the activity concentration in the analytical samples. A radionuclide with a high activity will result in many counts, as this nuclide will readily undergo radioactive decay. Hence, the counting time could be reduced. If a sample has a low activity, the radioactive decay occurs seldom. By increasing the counting time, a higher number of counts could be detected by the NaI-detector, and the standard error is reduced (Choppin, G., Liljenzin, J. O. & Rydberg, J., 2016). If the activity detected by the NaI-detector is below 10 times the standard deviation of measured blanks, the activity is below the quantification limit of the NaI-detector and the activity cannot be quantified. The quantification limit was ~10 and ~5 *cpm* for ^{134}Cs and ^{137}Cs, respectively. The HMM/colloidal fraction for both sorption and remobilization was, in general, below the quantification limit.

By increasing the counting time, the uncertainty could have decreased and a higher activity (dpm) might been acquired. However, in this thesis, the change in the speciation distribution was important to monitor and not the exact activity concentration in each sample replicates. The tracer activity added to the riverine colloid and clay suspensions as well as the saline water was dependable to provide enough counts to assure that monitoring would be possible.

ICP-MS was employed to determine the amount of stable Cs (^{133}Cs) in the experimental waters. Since stable Cs will compete with the radiocaesium, it is important to have knowledge about the amount of stable Cs in the system. The quantification limit (LOQ) of ^{133}Cs in freshwater was 6.0×10^{-4} *µg/L* and for saline water 6.0×10^{-3} *µg/L*. The LOQ for saline water is higher, due to a 10 times dilution of the samples. The detection limit (LOD) for freshwater and saline water was 2.0×10^{-4} and 2.0×10^{-3} correspondingly. The LOD and LOQ were calculated to 3 times and ten times the standard deviation of the blank samples, respectively. The measurements were within <1 % of the certified value of the standard used (NIST 1640a).

4.2 Water chemistry

Table 3 gives an overview of the chemistry of different experimental waters used in the compartment systems.

Table 3: The chemical composition of experimental waters				
Parameter	<10*kDa* Storelva	<0,45*µm* Storelva (including HMM)	<10*kDa* Artificial Storelva water	<10*kDa* Saline water (LMM)
pH	6.43	6.63	6.17	7.8
Temperature (◦C)	20	20	20	20
Conductivity	41 µS/cm	51 µS/cm	32 µS/cm	58.3 mS/cm
TOC (mg/L)	3.9	5.8	0.36	2.0
Na(mg/L)	2.4	2.9	3.2	11000
Mg(mg/L)	0.74	0.63	0.62	1600
K(mg/L)	0.41	0.48	0.35	420
Ca(mg/L)	1.1	2.0	1.5	430
^{133}Cs (µg/L)	0.023	0.037	0.0061	0.30
Cl^- (mg/L)	5.2	4.8	0.3	42400
SO_4^{2-} (mg/L)	2.6	3.6	13	6300
NO_3^- (mg/L)	0.13	0.18	<0.02	12

The amount of stable Cs will influence the binding of radiocesium to colloids and clay minerals, as stable Cs will compete for available binding seats. This applies for K^+, Na^+, Mg^+ and Ca^+ as well. As expected, there is a high amount of competing ions in the saline water. There is also a higher amount of stable Cs in the saline water than the riverine water. Thus, assumed a higher competition of stable cesium with radiocesium in water of high salinity than at low salinity.

4.3 ^{134}Cs activity sorption to riverine colloids

The sorption of ^{134}Cs to riverine colloids from Storelva was investigated and the change in distribution of the tracer was followed by size fractionations. The distribution of the ^{134}Cs tracer is presented in figure 9. As the figure indicates, the Cs tracer was mainly associated with the LMM fraction in the riverine colloids (blue column). After 10 minutes, 2.5 % ^{134}Cs was associated with the riverine colloidal fraction, with an increase to 5 % after 5 months sorption

time. This indicates that the Cs tracer show a minor sorption to the colloidal fraction, and if sorption happens, the reaction is rapid (1 hour 4.4 %). The bar graph suggests that the sorption to the colloidal fraction decreases after 5 month, this result could be within the sampling and measurement uncertainty for the NaI-detector. During the 5 months, there was no detection of Cs in the >0.45 μm syringe filters, which means Cs was not associated with particles in the colloidal suspension. Visual observations on the syringe filters suggest that there were a small amount of colloids agglomerated into particles during the 5 months in freshwater. This experiment is ongoing as a part of another study and further analysis will not be included in this thesis.

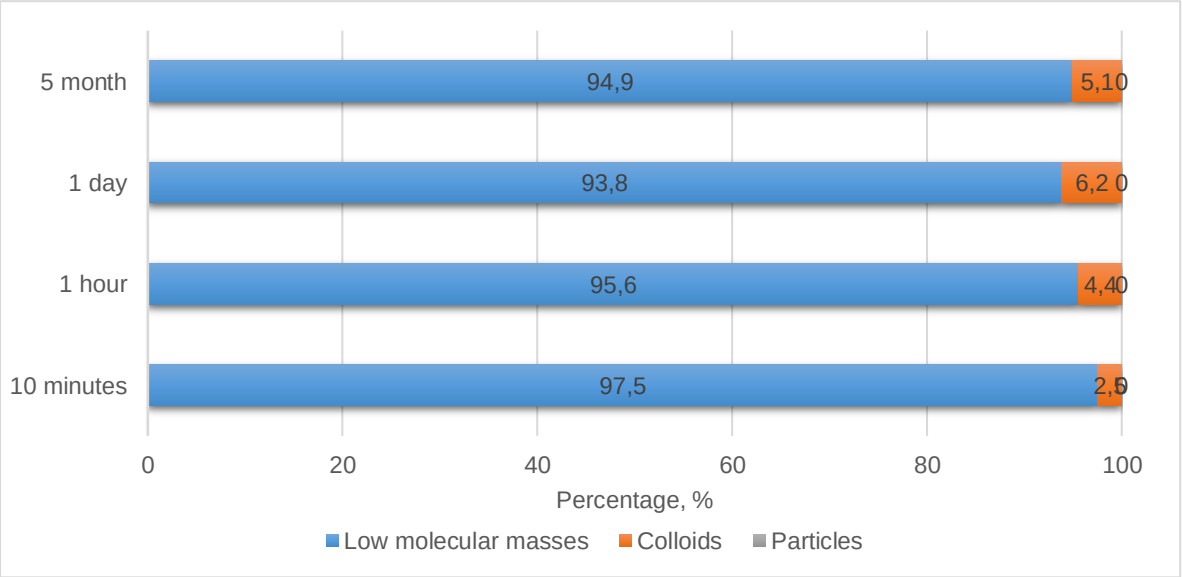

FIGURE 9 SHOWS THE RELATIVE (%) DISTRIBUTION OF ^{134}CS ASSOCIATED WITH THE LMM, COLLOIDAL AND PARTICLE FRACTION. DURING THE 5 MONTHS, 5 % ^{134}CS HAD SORBED TO THE RIVERINE COLLOIDS FROM STORELVA. THERE WAS NO AGGREGATION OF COLLOIDS INTO PARTICLES.

4.4 Salinity dependent remobilization of ^{134}Cs from riverine colloids

Remobilization of ^{134}Cs from riverine colloids from Storelva was tested with regards to gradient saline brackish water. To ensure removal of the ^{134}Cs tracer associated with the LMM fraction in the riverine colloidal suspension, the colloidal suspension went through a washing procedure using artificial Storelva water. This washing procedure proved to be too efficient, as it caused remobilization of the ^{134}Cs tracer associated with the colloidal fraction in the suspension. This washing step has been illustrated in figure 10 were the colloidal suspension with tracer were washed successively with MilliQ water, artificial riverine water and saline water with *PSU* 30 (5mL of tracer colloidal suspension washed with 5 mL, 5 times). As the figure demonstrates, washing with 25 mL of water (5 times dilution), regardless of water quality, remobilized the tracer.

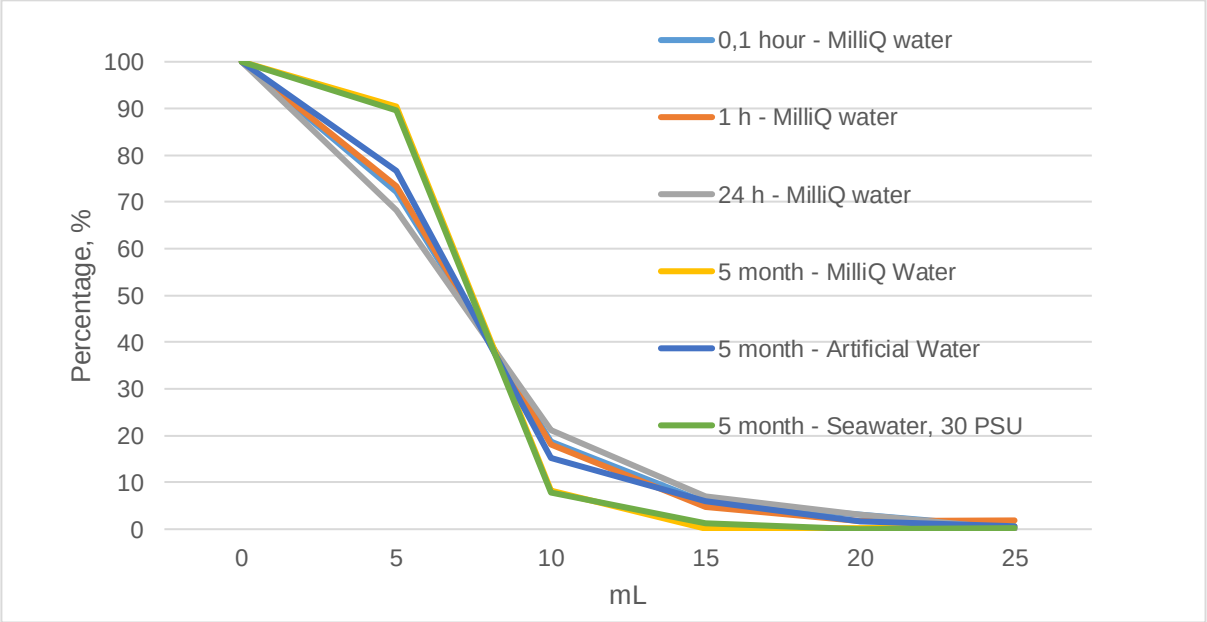

FIGURE 10 SHOWS THE SUCCESSIVELY WASHING OF THE CESIUM COLLOIDAL SUSPENSION WITH MILLI Q WATER, ARTIFICIAL RIVERINE WATER AND SALT WATER WITH PSU 30. AFTER WASHING WITH 25ML, THE TRACER HAD REMOBILIZED.

Even though there were low levels of ^{134}Cs tracer left in the colloidal suspension, the experiment proceeded, and the colloidal suspension was added gradient saline brackish water. As indicated in figure 11 on the next page, the ^{134}Cs tracer showed a clear association with the LMM fraction (95-100 %) and some association with the HMM (0-1%) and the >0.45 μm fraction (2-5%) for all salinities for the entire period of the experiment. This indicates that if ^{134}Cs associates with riverine colloids, Cs will easily mobilize due to either 1) an increase of river-water with lower concentrations of Cs, which leads to a dilution or 2) in the presence of brackish saline water, which introduces competing ions.

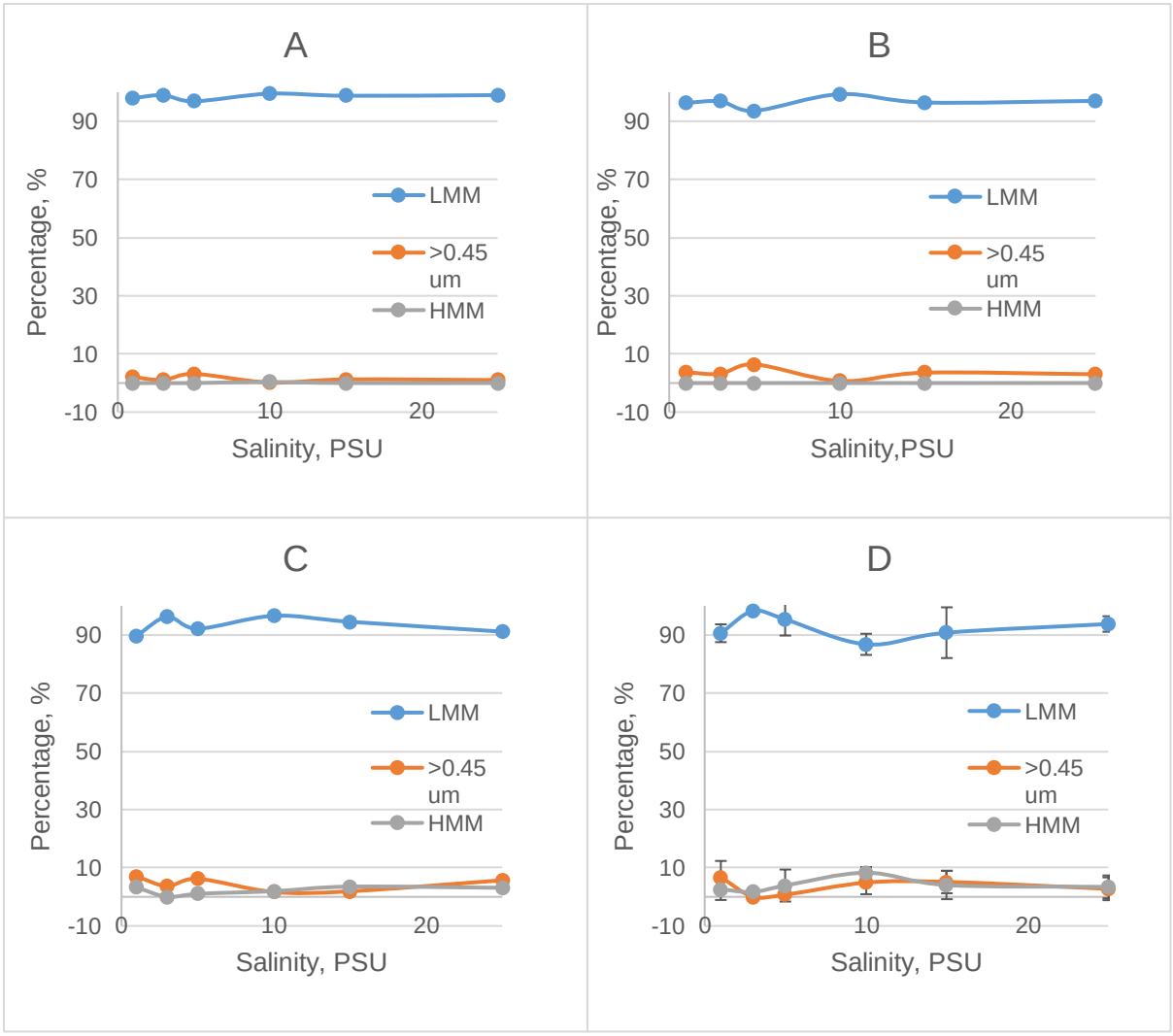

FIGURE 11 SHOWS THE RELATIVE (%) DISTRIBUTION OF ^{134}CS AT A: 5 HOURS, B: 24 HOURS, C: 8 DAYS AND D: 1 MONTH WITH GRADIENT SALINITY (1, 3, 5, 10, 15 AND 25 PSU). AT EXTRACTION TIME 5H, 24H AND 8 DAYS THE STANDARD DEVIATION IS NOT GRAPHICAL VISUAL, AS FOR 1 MONTH THE STANDARD DEVIATION INCREASED, THIS IS DUE TO AN INCONSISTENCY IN RESULTS FROM THE NAI-DETECTOR FOR EACH SAMPLE REPLICATE.

As the binding of Cs to colloids occurs through ion exchange (Cornell, R., 1993), and the electron affinity of Cs is less than other ions (K^+ and Na+) (Myers, R. T., 1990). Cs is not readily attracted to the colloids. The degree of Cs binding to colloids is affected by the presence of other competing ions, the number of binding seats available for cesium on the colloid, available humic material functional groups for complexation reactions and water chemistry like pH and salinity (vanLoon G. W. & Duffy S.J., 2011). Even though Cs not readily sorbs to riverine colloids, some association should be expected. This factor is important in risk assessments. If there are some Cs association to colloids, this association will most likely

disrupt the moment the colloids enters brackish waters or in periods with high precipitation or snow melting that leads to an alteration in the water chemistry and a dilution of the Cs concentration in water. When this association disrupts, a local increase in LMM Cs^+ ions are expected although elevated dilution processes are ongoing in estuaries (Teien et al., 2006; Machado et al., 2016; Sanial et al., 2017).

The standard deviation increased at the 1-month extraction time. The counting of the colloidal and particle fraction by the NaI-detector showed clear inconsistencies (Appendix C). This could indicate that the samples were heterogeneous. However, it is difficult to conclude as the activity in some samples were below the quantification limit of the NaI-detector.

Tracer activity detected in the syringe filters (>0.45 μm) indicates some agglomeration of colloids into particles. This activity was however very low. There was a slightly indication that agglomeration in the lower salinities were higher and that this trend increases by time. Particle growth (*brownish strands*) was visually observed in some of the sample replicates.

4.5 Salinity dependent sorption of ^{137}Cs ions to riverine colloids

^{137}Cs present as ions in saline water was added to the riverine colloids to study the sorption of radioactive cesium to riverine colloids as a function of gradient salinity. Figure 12 gives a presentation of the activity (*dpm*) of ^{137}Cs associated with the riverine colloids after one-month sorption time with gradient salinity.

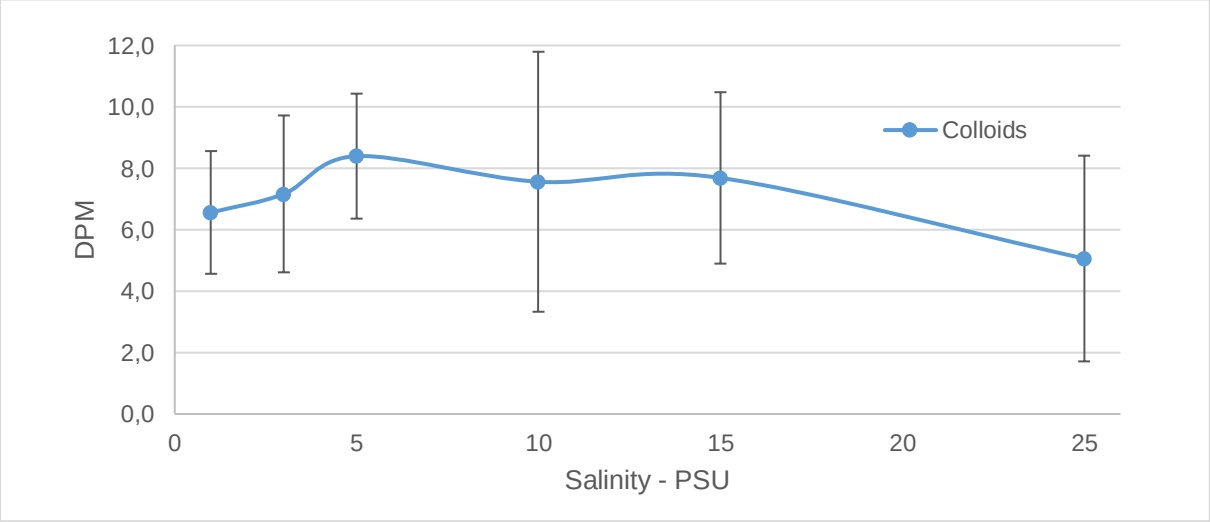

FIGURE 12 THE MEASURED ACTIVITY (DPM) OF ^{137}CS ASSOCIATED WITH RIVERINE COLLOIDS AFTER ONE-MONTH SORPTION TIME AS A FUNCTION OF GRADIENT SALINITY.

As the figure demonstrates, there were some ^{137}Cs association with the riverine colloids. The figure indicates that the ^{137}Cs association with colloids were highest at salinity 5 PSU, although uncertainties are rather high. The measured activity (*dpm*) of ^{137}Cs associated with the colloids in the 5 *PSU* sample are graphical represented as a function of time (Fig. 13).

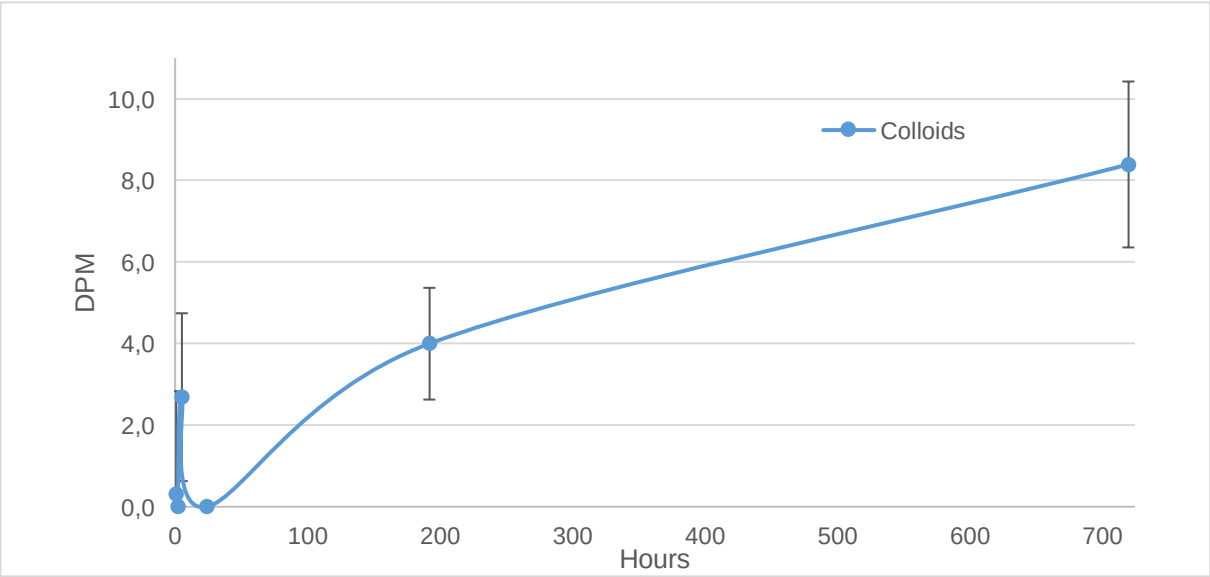

FIGURE 13 THE MEASURED ACTIVITY (DPM) OF ^{137}CS ASSOCIATED WITH RIVERINE COLLOIDS AT 5 PSU WITH A ONE-MONTH SORPTION TIME.

The figure clearly demonstrates that after one-month sorption time, there was an increase of Cs associatied with riverine colloids in brackish water with a salinity of 5 *PSU*. Even though the measured activity was minor, and most ^{137}Cs was associated with the riverine LMM fraction (Appendix D), in risk assessments and models this evident relationship must be accounted for. As mentioned before, if riverine colloids contaminated with Cs enters high salinity waters, hence, introducing a high amount of competing ions to the colloids, the Cs would most certain be desorbed from the particle surface. This will lead to a local increase of LMM Cs^+ ions even though there is a high degree of dilution in estuaries (Teien et al., 2006; Machado et al., 2016; Sanial et al., 2017). As uptake and accumulation of the LMM species in biota are of most concern, (Teien *et* al., 2006; Carvalho, 2018), it is important to take into account the Cs association with both colloids as well as particles in risk assessments and models. If not accounted for, this could lead to an underestimation of the amount of contaminants present in river-ocean systems.

4.6 ^{134}Cs activity sorption to riverine clay

The isolated riverine clay fraction was also added ^{134}Cs to study the sorption of Cs to clay. The sorption of ^{134}Cs to the clay displayed a different image than for the colloids. As figure 14 reveals, 98.8 % of the ^{134}Cs tracer was sorbed to the riverine clay after only one day. After 5 month, the sorption of ^{134}Cs to clay reached 99%, indicating that the sorption of Cs to clay was rapid and effective in freshwater qualities similar to Storelva. The degree of binding to the clay (irreversible, fixed, e.g.) is not obtained from size fractionation techniques. Thus sequential extraction would provide information about this (Oughton et al., 1992; Skipperud, L. & Salbu, B. 2015). However, this was not the scope in this thesis.

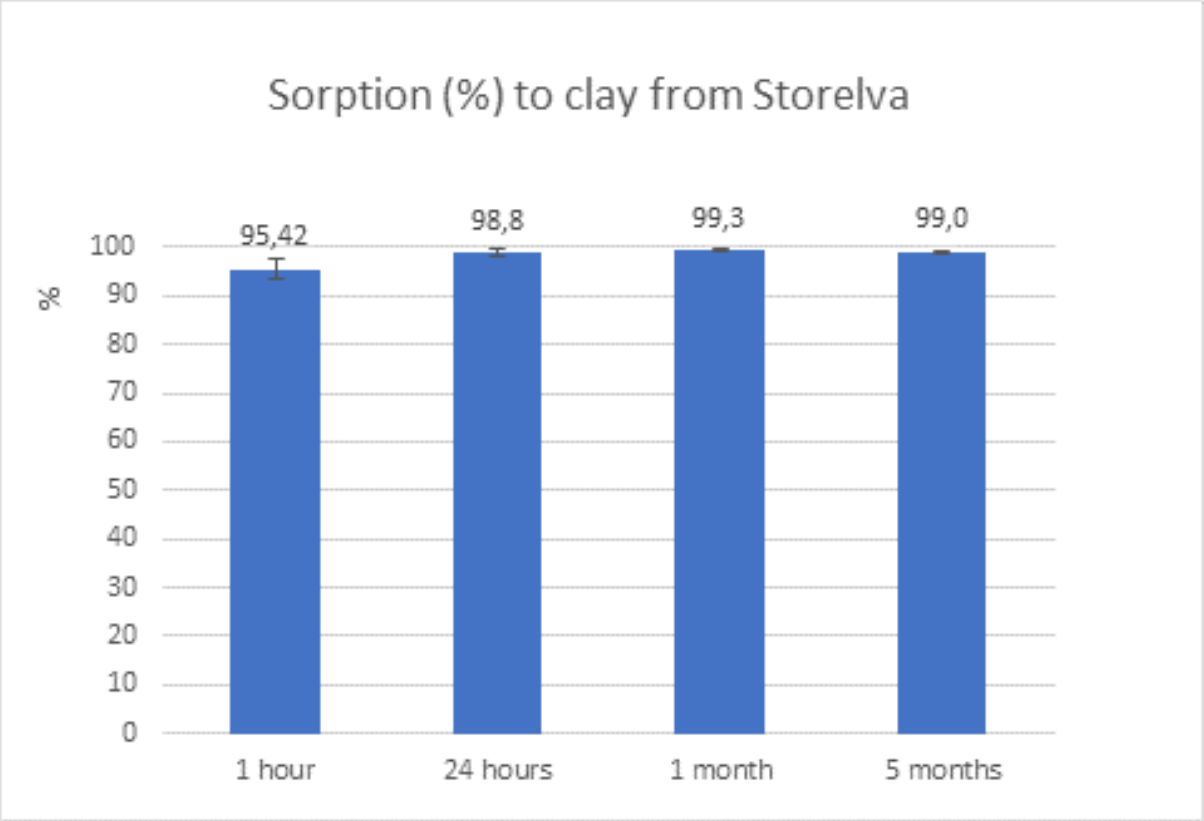

FIGURE 14 SORPTION OF ^{134}CS TO RIVERINE CLAY FROM STORELVA WITH CONTACT TIMES 1 HOUR, 24 HOURS, 1 MONTH AND 5 MONTHS. AFTER 5 MONTH THE SORPTION TO CLAY WAS 99 %.

There were no findings of ^{134}Cs association with the colloidal fraction, as the remaining fraction was associated with the LMM fraction in the Storelva clay suspension.

4.7 Salinity dependent remobilization of ^{134}Cs from riverine clay

Riverine clay was added brackish water with gradient salinities to study the remobilization of ^{134}Cs. Prior to this, the same washing procedure with artificial water was performed on the clay freshwater suspension as for the colloids, the remobilization of ^{134}Cs from clay was minimal compared to the riverine colloids.

Figure 15 gives a presentation of the relative (%) distribution of ^{134}Cs associated with the LMM and particle (>0.45 μm) fraction for each salinity as a function of time. Figure 16 present the same data, but gives the relative distribution of ^{134}Cs associated with the LMM, HMM and particles (>0.45 μm) for each extraction time as a function of salinity. The HMM fraction was excluded in figure 15, as the ^{134}Cs associated with the HMM fraction was minor (0-1 %) as indicated in figure 16. This could be due to absence of the colloidal fraction in the riverine clay suspension, resulting in no colloidal fraction in the solution to offer binding seats for Cs or that the HMM colloidal fraction was aggregating to size fractions larger than 0.45 μm.

Figure 15 demonstrates that the remobilization of ^{134}Cs associated with clay increased by time. This trend was also a function of the increasing salinity. After 24 hours, nearly 40 % ^{134}Cs was associated with the LMM fraction for all salinities. After 8 days and at 25 *PSU*, there was more ^{134}Cs associated with the LMM fraction than the clay fraction. After 1 month, this appeared at 10 and 15 *PSU* as well. As for the lower levels of salinity (1, 3 and 5 *PSU*), there were more ^{134}Cs associated with the clay throughout the experiment. This demonstrates that Cs associated with riverine clay can remobilize as a function of an increase in salinity and time. The higher salinities, the more Cs remobilized.

Figure 16 also demonstrates that with an increase in both time and salinity the remobilization of ^{134}Cs from clay increases, and the remobilization was faster.

This means that if riverine clay containing Cs discharges to the coastal water, Cs^+ can remobilize from the clay. When riverine clay enters saline waters, an increase in competing ions appears (K^+, Na^+ and Ca^+ as well as stable Cs^+). This results in an increased ionic strength of the solution. K^+ has an especially high affinity to clay, as K^+ ions are commonly found in clay minerals, binding the interlayers together (Børrentzen P., Salbu B. 2002). This result in tracer Cs^+ ion exchanging with K^+ (or stable Cs), leaving Cs^+ ions kept free in solution.

When riverine water meets coastal water, dilution occurs. Riverine particles, like colloids and clay, will undergo sedimentation in estuaries due to a decrease in the water-flow. Due to their small size, the LMM fraction would disperse with ocean currents. This again leads to dilution of the LMM fraction. As demonstrated with models and environmental monitoring programs (RAME, 2017), detection of radionuclides discharged to the marine environment from far distances are possible along the Norwegian coastline. This clearly shows that the LMM fraction has the ability to travel a far distance with the ocean currents, and can then induce harm at other locations than discharge origin.

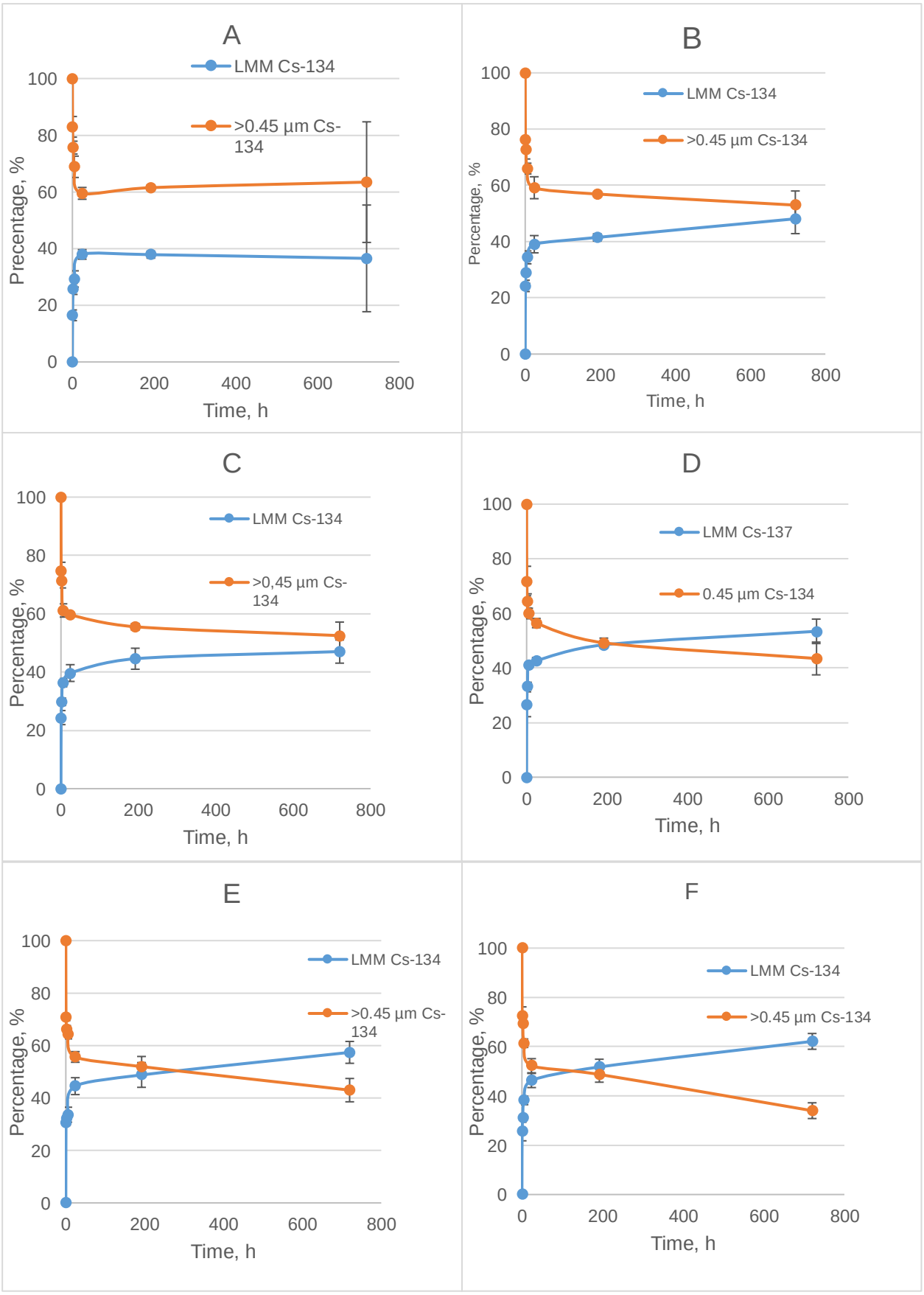

FIGURE 15 REMOBILIZATION OF ^{134}CS FROM RIVERINE CLAY AS A FUNCTION OF TIME AND AT DIFFERENT SALINITIES: A IS 1 PSU, B IS 3 PSU, C IS 5 PSU, D IS 10 PSU, E IS 15 PSU AND F IS 25

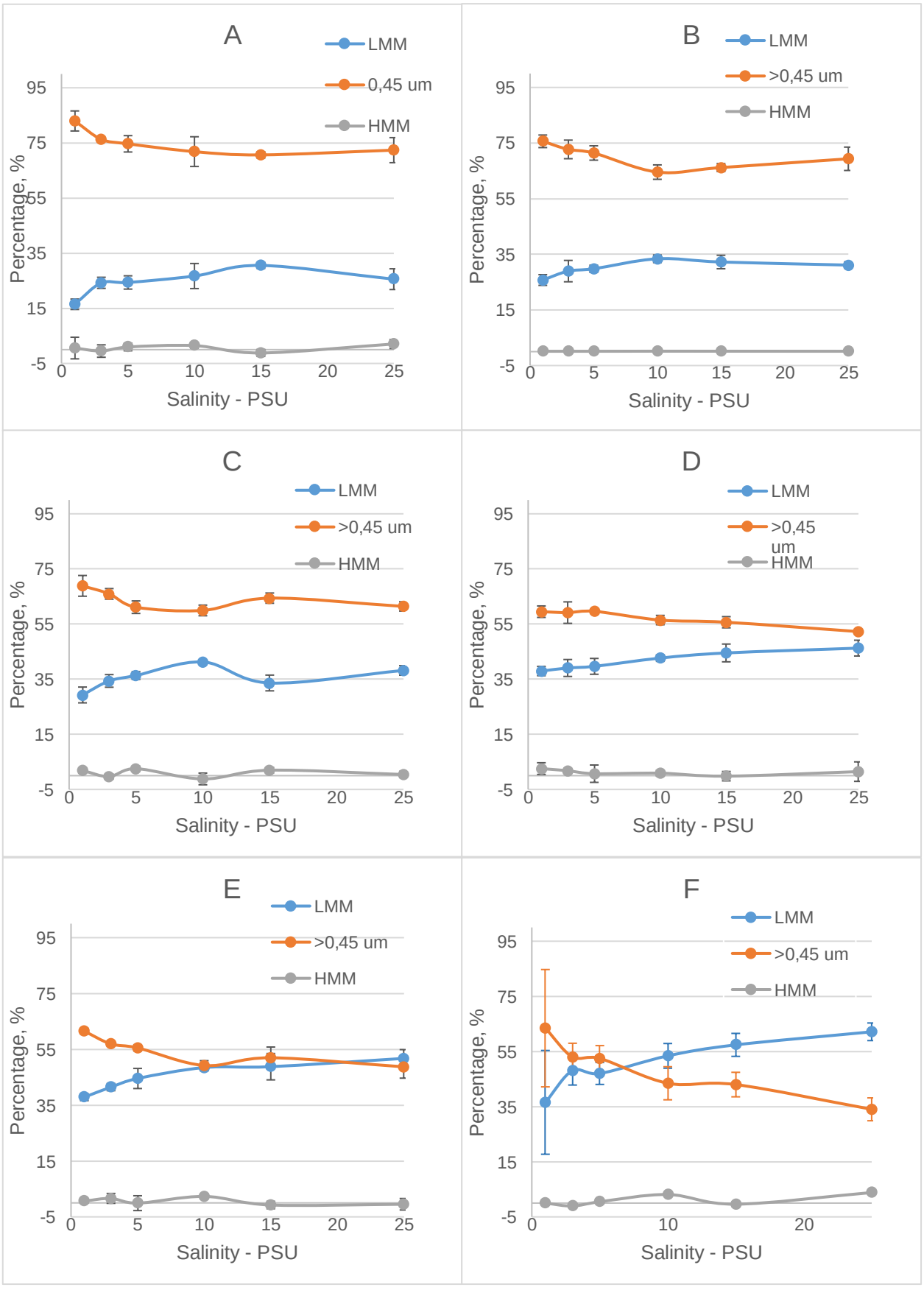

FIGURE 16 REMOBILIZATION OF ^{134}CS FROM RIVERINE CLAY AS A FUNCTION OF SALINITY AT DIFFERENT EXTRACTION TIMES: A IS 0,5 H, B IS 2 H, C IS 5 H, D IS 24 H, E IS 8 DAYS AND F IS 1

4.8 Salinity dependent sorption of ^{137}Cs ions to clay

^{137}Cs present as LMM species in saline water was mixed with freshwater clay to study the sorption of radioactive cesium. Figure 17 gives the relative (%) distribution of ^{137}Cs for each salinity as a function of time after mixing, while figure 18 gives the relative (%) distribution of ^{137}Cs for each extraction time as a function of salinity. After 1 month there was more ^{137}Cs associated with the clay fraction (>0.45 μm) than the LMM fraction at salinity 1 *PSU*. At salinities above 1 (3, 5, 10, 15 and 25 *PSU*) and at all extraction times (2h, 5h, 24h, 8 days and 1 month) there was more ^{137}Cs associated with the LMM fraction than with clay. At 3 and 5 *PSU*, after 1 month about 40 % ^{137}Cs was associated with the clay fraction (>0.45 μm) as for 10 *PSU* there were only 25 %. For 25 *PSU* after 1 month, there were only 9 % associated with the clay. This indicates that the sorption is salinity dependent and increases with decreasing salinity.

At salinity 1 *PSU*, 20 % of the ^{137}Cs ions had sorbed to the riverine clay after 0.5 hours. After 1 month, the sorption increased to 54 %. The graph indicates that if the experiment had gone on for a longer time, the sorption of ^{137}Cs to clay had increased even more. However, the standard deviation for 1 *PSU* at extraction time 1 month was very high. This was due to inhomogeneous samples, with very little clay left in two of the sample replicates. These were clear outliers and correction for this was made in the graph. For all other salinities, the standard deviation indicates that there was a good correlation between the replicates.

In this experiment, obviously, there were a competition between the two tracers ^{134}Cs and ^{137}Cs, over the available binding seats on the clay mineral. As the binding seats might already been occupied by ^{134}Cs, this could lead to a lower sorption of ^{137}Cs to the clay.

The results demonstrated that if ^{137}Cs are present as ions in saline water, sorption to riverine clay occurs, but the sorption is highly dependent upon salinity, contact time and the presence of competing ions (e.g. Na^+, ^{134}Cs). In general, the sorption increased with increasing contact time and decreasing salinity.

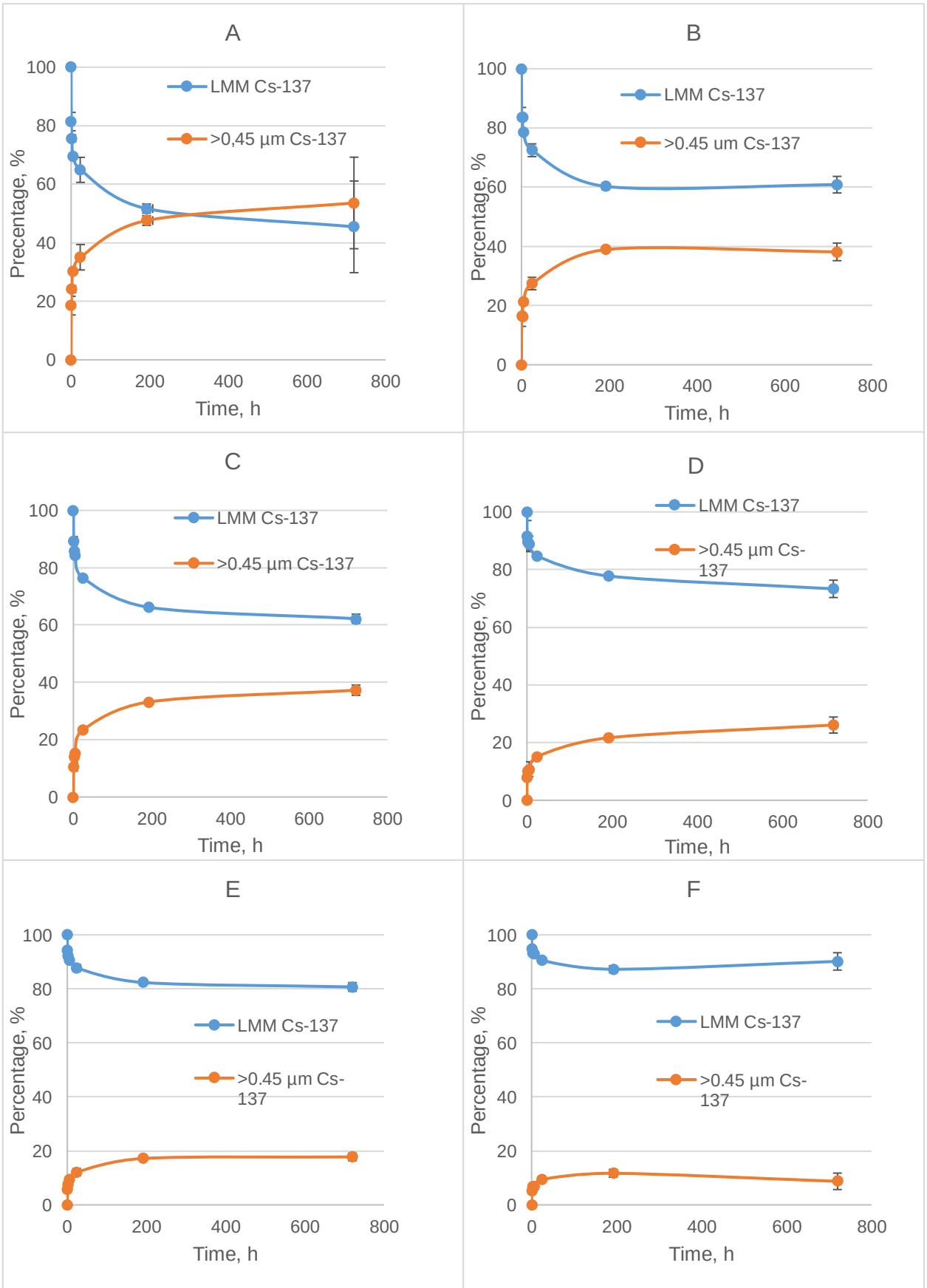

FIGURE 17 SORPTION OF ^{137}CS IONS FROM SALINE WATER TO RIVERINE CLAY AS A FUNCTION OF TIME AT DIFFERENT SALINITIES: A IS 1 PSU, B IS 3 PSU, C IS 5 PSU, D IS 10 PSU, E IS 15 PSU AND F IS 25 PSU.

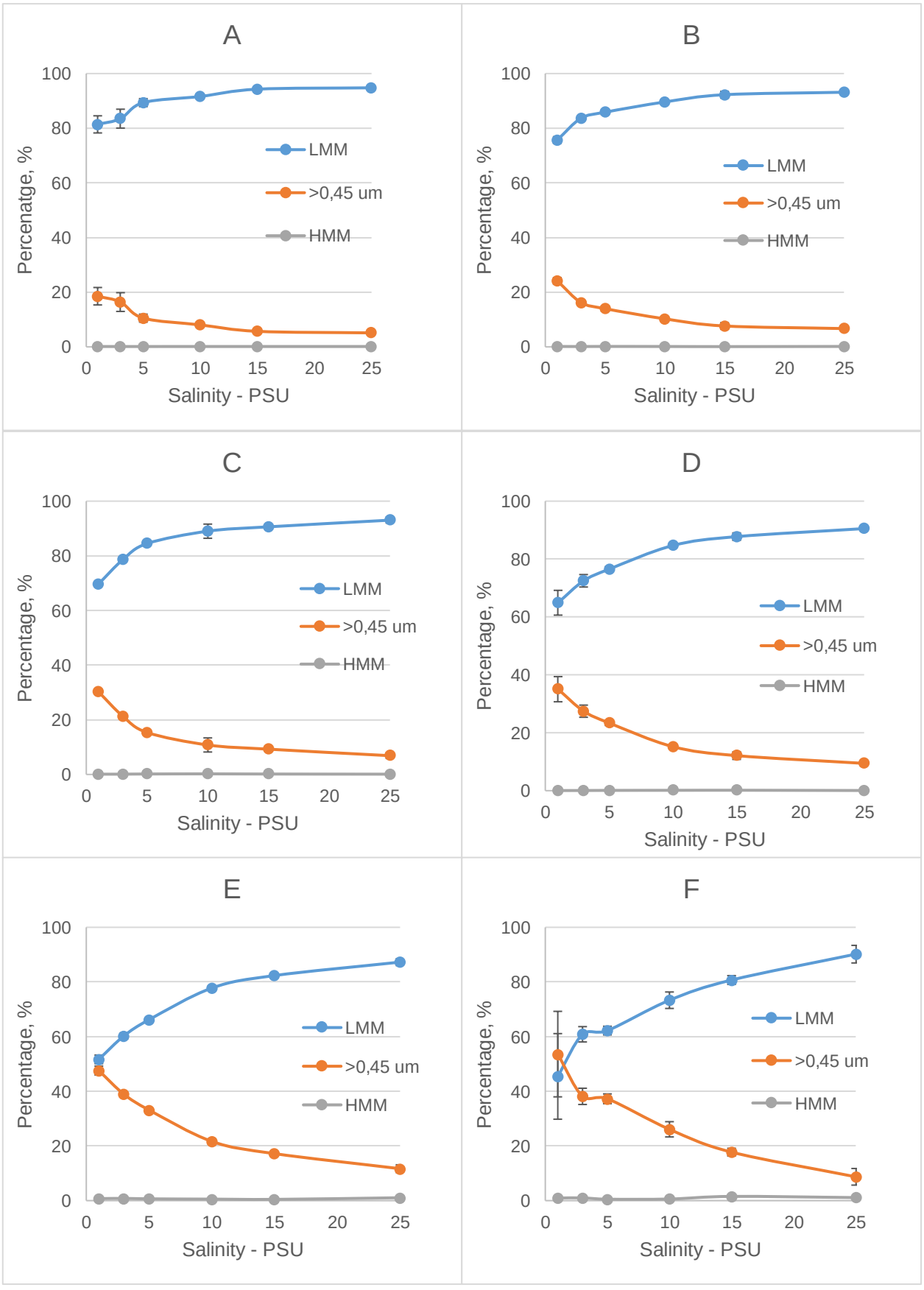

FIGURE 18 SORPTION OF ^{137}CS IONS FROM SALINE WATER TO RIVERINE CLAY AS A FUNCTION OF SALINITY AT DIFFERENT EXTRACTION TIMES: A IS 0,5 H, B IS 2 H, C IS 5 H, D IS 24 H, E IS 8 DAYS AND F IS 1 MONTH.

As indicated in figure 18, ^{137}Cs showed no sorption to the riverine HMM fraction. However, at 8 days and 1 month there was detection of trace amounts (Appendix C).

4.9 Size distribution dependent upon source

The ^{134}Cs tracer originated from the riverine clay and the ^{137}Cs tracer from the saline water. When comparing the LMM association for both tracers at all salinities after 1 month, there was a lower amount of ^{134}Cs associated with LMM than ^{137}Cs. This indicates that the source origin of the tracer matters. It can also indicate that some ^{134}Cs has a degree of fixation to the clay, as maximum of ~60 % could remobilzed from the clay (25 *PSU* after 1 month). The experiment lasted for 1 month, there could be a possibility that the remobilization of ^{134}Cs from the clay would have continued if conducting the experiment for a longer period. As demonstrated in figure 15, the remobilization of ^{134}Cs showed an increasing tendency after 1 month, except for the salinity 1 *PSU*. At this salinity, a state of equilibrium was suggested. This was also the case for the ^{137}Cs tracer, where figure 17 indicates a state of equlibrium at higher salinity levels (15 and 25 *PSU*), while the sorption to clay was still increasing at low salinity levels. In addition, a competition between the two tracers over avaliable binding seats on the clay mineral should not be ignored. However, the radioactive tracers represents minute amount of atoms compared to stable Cs in waters (Salbu,

4.10 Apparent *Kd* as a function of salinity

The distribution of Cs did not reach equilibrium in this experiment. That is why the apparent *Kd* is presented. Figure 19 and table 4 show the apparent *Kd* obtained for clay and water at different salinity. Appendix F contains the experimental data.

Table 4: Apparent *Kd* range determined for ^{134}Cs and ^{137}Cs at different salinities. The unit for K_d is Lkg^{-1} (dw)

Salinity - PSU	^{134}Cs	^{137}Cs
1	215	160
3	147	84
5	150	79
10	107	47
15	99	29
25	73	13

The K_d was calculated by using the dry weight (dw) of clay. Due to the small amount of clay in each syringe filter, it was not possible to determine the weight of the actual amount of clay for each sample replicate. Hence, the weight of clay used in the K_d calculations was based on gram clay per ml solution (see section 3.3 in method and materials). However, due to inhomogeneous samples, a large uncertainty to this method was detected. Recommended K_d values for Cs is 2.9 $x10^4 Lkg^{-1}$ in freshwater and 2 $x10^3$ Lkg^{-1} in saline water (IAEA, 2004; IAEA, 2010). These K_d values suggest orders of magnitude higher values than the K_d values obtained in this experiment. This could be due to an overestimation of the amount of clay in each replicate. Since the apparent K_d values are much lower than recommended K_d values, and there is a high uncertainty in the determination of the weight of the clay, the obtained K_d values should be used with care. However, the relative changes of K_d due to the increase in salinity can be used.

In addition, it is important to recognize that the recommended values given by IAEA are for Cs in freshwater or saline water and are under equilibrium conditions. This experiment was conducted in brackish waters and equilibrium conditions during the one-month period were not achieved. However, the K_d values obtained in this experiment should be expected in between the recommended K_d values.

As mentioned in the introduction, a high K_d indicates that the element is particle-reactive or non-conservative. Meaning that the element shows a higher fixation to the sediments, which leads to a low mobility. A low K_d means there is an increase in the mobility and the element is conservative (i.e., non-reactive), meaning it is kept in solution. The K_d obtained in this experiment indicates a decreasing values when the salinity increased by a factor of 3 for ^{134}Cs and 2 for ^{137}Cs. The change in K_d with increasing salinity clearly demonstrates that *Kd* is highly dependent on site-specific conditions.

The *Kd* is said to be time dependent. As demonstrated in the figures below, the *Kd* will change with time until equilibrium condition is reached. These alterations are important to recognize, as they will make it easier to understand why a system is in constant change. Ion-exchange properties effects the system, as Cs will both sorb and desorb at the same time. The interaction or contact time between Cs and clay is important, as this can ultimately lead to a fixation of Cs in the interlayer clay mineral.

As demonstrated by Børrentzen and Salbu (2002), sequential extraction can be utilized to evaluate the degree of binding of Cs in clay. This technique used water and chemicals with different extraction strength. The stronger extraction chemicals needed to break the bindings

the higher degree of fixation to the clay are expected. In this experiment, after one year of contact time between tracer and clay, the tracer was regarded fixed, and could not be extracted. At this point, a state of equilibrium or at least pseudo-equilibrium was obtained.

Equilibrium condition in nature is hard to achieve, as water-sediment systems are in constant change (water flow, waves, precipitation, sedimentation, particle growth, weathering of sediments during storms e.g.). In this work, closed compartment systems without external influence were employed. If the experiment had been conducted for a longer period, a state of equilibrium might have been achieved.

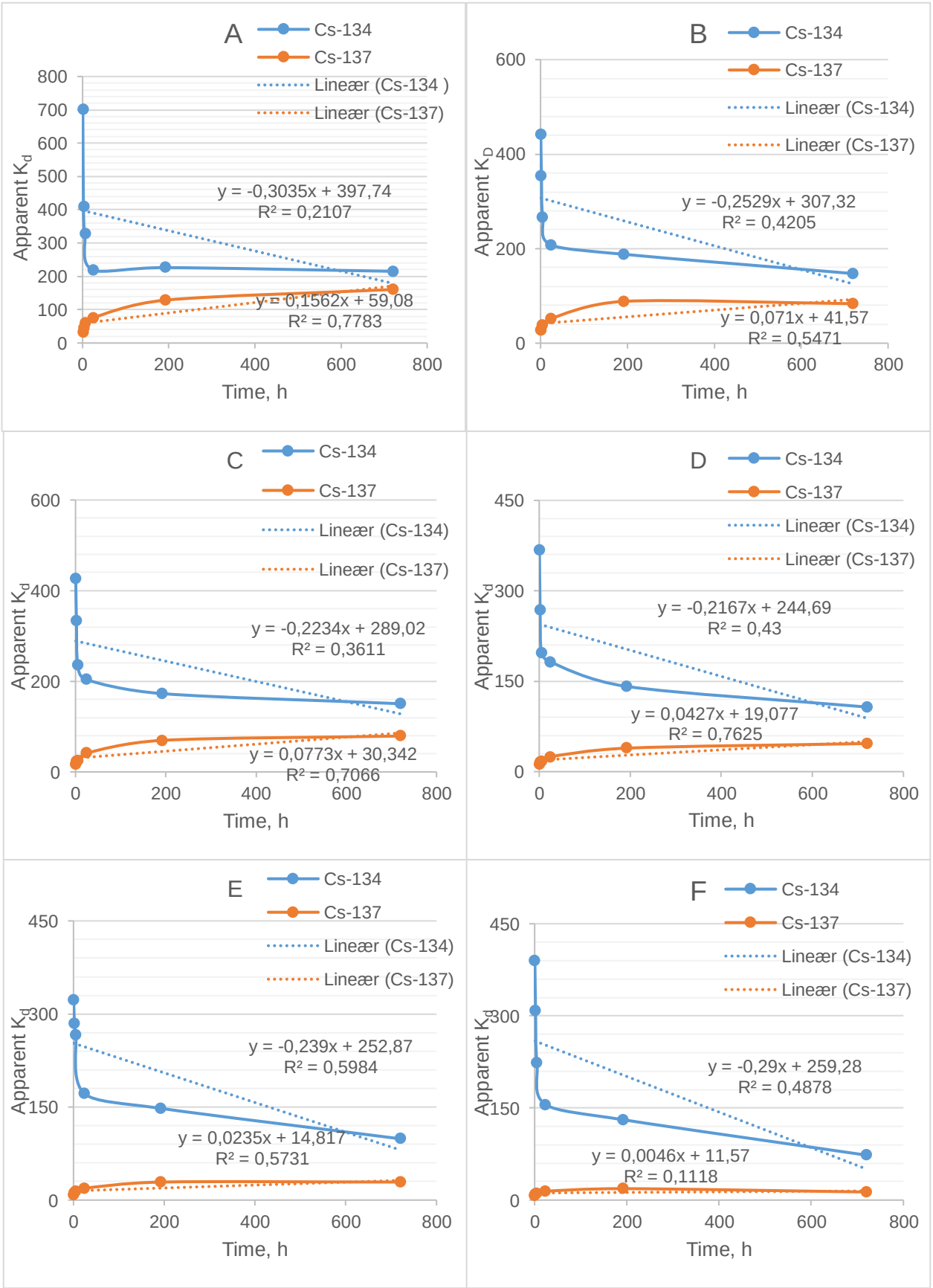

FIGURE 19 APPARENT KD FOR ^{134}CS AND ^{137}CS AS A FUNCTION OF TIME FOR WATERS WITH DIFFERENT SALINITIES: A IS 1 PSU, B IS 3 PSU, C IS 5 PSU, D IS 10 PSU, E IS 15 PSU AND F IS 25 PSU.

4.11 Transfer rates

The estimated sorption and desorption rates are presented in table 5 and 6 respectively. Appendix G gives an overview of the methodology and results for the calculations of transfer rates.

Table 5: The estimated transfer rates from the ^{137}Cs sorption data. Units of the transfer rates are s-1.		
Salinity -*PSU*	k1	k2
1	4.448×10^{-6}	3.771×10^{-6}
3	3.804×10^{-6}	6.069×10^{-6}
5	3.124×10^{-6}	5.217×10^{-6}
10	1.734×10^{-6}	4.872×10^{-6}
15	1.452×10^{-6}	6.608×10^{-6}
25	1.717×10^{-6}	1.777×10^{-6}

Table 6: The estimated transfer rates from the ^{134}Cs remobilization data. Units of the transfer rates are s-1.		
Salinity - *PSU*	k1	k2
1	-	-
3	7.354×10^{-6}	6.679×10^{-6}
5	8.331×10^{-6}	7.462×10^{-6}
10	5.742×10^{-6}	7.056×10^{-6}
15	5.217×10^{-6}	6.964×10^{-6}
25	4.174×10^{-6}	7.623×10^{-6}

Results show that both the sorption and desorption rates are in the same magnitude in brackish water of low and high salinity. In general, the sorption rates (*k1*) seems to decrease by salinity by a factor of 2, while the desorption rates (*k2*) are not dependent upon salinity. The distribution of Cs is, however, dependent upon salinity, thus the time to reach equilibrium will depend upon salinity.

The estimated transfer rates utilized in a kinetic model could give an estimate of the dispersal of Cs in Storelva and into the Sandnesfjord. In case of an adverse event with a release of radiocesium, utilizing this model could be a useful tool for deciding on countermeasures or in a risk assessment perspective, to plan for adverse events.

5 Sources of errors

The concentration of stable Cs was not quantified in the riverine clay. Stable Cs could interfere with the sorption to clay for both tracers, as stable Cs will occupy binding seats on the clay. This could lead to a lower degree of sorption for the tracers towards the clay. However, the amount of clay present in the experiment was thought to offer sufficient binding seats for both tracers, hence the concentration of stable Cs in clay was neglected.

The ^{137}Cs was added each sample replicate by pipette (100 µl). This could give a variation in the activity among replicates, and increase the standard deviation of the mean. The activity of the tracer determined by the NaI-detector was also included in the evaluation of the accuracy of the pipetting. The variation of this pipetting was approximately 1 %. It is eligible to believe that the same uncertainty will apply for the mentioned above sampling.

When extracting samples, the distribution of clay in the suspension showed an uneven distribution. Samples were collected with syringe from the suspension, and the content of clay in each collected sample was not constant. This became clear for the samples extracted after one month. The syringe filters were weighed empty and with clay to determine the clay content in each sample and to normalize the data. However, the weight of clay was only minor compared to the weight of the filter making this estimate uncertain. For some of the syringe filters the tared weight came out negative. Some samples became clear outliers due to visual observations of small clay amounts and a low counting result on the NaI-detector compared to equal replicates. Due to this, clear outliers were removed, as they affected the presentation of the results.

The K_d values obtained for Cs in this experiment were much lower than reported K_d values for Cs. This could be due to an uncertainty in the determination of amount clay in each sample replicate.

When centrifuging samples, some of the fluid did not pass the centrifugal filter. There was a small residue in fraction (*>10 kDa*). The residue would have been analyzed as the HMM fraction, but could likely be LMM or a mix of HMM and LMM, the residue was therefore removed. Thus, it could lead to an overestimation of measured activity in the HMM fraction. The residue was not retained, nor analyzed on the NaI-detector and is therefore unaccounted for. In fact, the fraction of LMM should thus be slightly underestimated.

Working with tracers, some common errors are necessary to take into account. Number one is the half-life of the tracer and number two is loss of tracer during sample preparation. The half-life of both Cs tracers is relatively long (2 and 30 years) so for most sorption experiments (months to years) the half-life of ^{134}Cs must be accounted for. This experiment is still ongoing. When washing the clay and colloidal suspension with artificial water, some leakages due to damaged tubes caused some loss of tracer. Loss of tracer can also happen due to the tracers' ability to sorb to surfaces like for instance the centrifugal tubes or syringes.

6 Suggestion to further investigations

The sorption study of ^{134}Cs to clay and colloids are ongoing. To obtain more results and to conclude whether the sorption to colloids decreases or increases by time, this experiment still needs following up. As results indicate so far, there seems to be a small decrease in the sorption.

The actual amount of clay present in the syringe filters should be determined, and the K_d values obtained in this thesis should be corrected for the actual amount of clay present in each sample replicate. This would reduce the uncertainty regarding the weight determination of clay and might provide more accurate K_d values.

To better achieve information on K_d under equilibrium conditions, the sorption and remobilization experiments should last for longer periods to prove if the calculated K_d is correct.

To evaluate the degree of binding of ^{134}Cs to clay, sequential extraction should be utilized. This would provide information about ^{134}Cs fixation to clay in estuarine waters. Thus improving the model, not only containing a two-box model, but a three-box model; dissolved, reversible sorption to particles and irreversible sorption to particles.

Further investigations of establishing methods to obtain information on Cs associated with the HMM fraction is also needed, as this were not fully obtained in this experiment.

In this master thesis, radioactive Cs tracers were used and the results obtained will provide useful information regarding transfer rates for Cs implemented into the transfer model developed by Simonsen et. al. (2019). Further research using other tracers or trace metals with different physico-chemical properties would give useful input information to the transfer model. For instance, experiments regarding element speciation of cadmium (Cd) would be useful, as there are still substantial levels of Cd in the terrestrial environment due to industrial activities (Norwegian Environmental Agency, 2017) that could impose a risk to the estuaries and the marine environment due to river run-offs.

7 Conclusion

The overall goal of this master thesis was to establish information on the transfer of Cs species in fresh waters to coastal areas. Hence, the work would focus on the dynamic water-sediment distribution coefficients and transfer-rates of Cs species as a function of salinity.

The hypotheses was:

H0: The distribution coefficient (K_d) of Cs between radioactivity in water and sediment is dynamic and dependent on salinity and will vary in brackish water with increasing salinity.

H1: Remobilization of Cs from river transported colloids and particles is more prominent for the marine transport than sorption of Cs to surfaces in saline waters.

7.1 Assessments of the hypothesis

H0 was supported, as the distribution coefficient (K_d) wass clearly dynamic and highly site specific. The distribution of Cs, both remobilization and sorption, changed by time. The salinity was a direct cause to an increase in the remobilization of ^{134}Cs from clay, and clearly interfered with the sorption of ^{137}Cs to clay. The distribution of Cs changed when the surroundings changed; an increase in salinity caused an increase in remobilization, and a decrease in the sorption.

H1 was supported, as the sorption of Cs to surfaces in saline waters was lower than the remobilization due to the presence of competing ions. The sorption was at is minimum due to the high levels of competing ions in saline waters. When Cs associated with riverine colloids or particles transports to the ocean, remobilization will occur due to the increase of competing ions. This will increase the concentration of LMM Cs^+ ions. As uptake and accumulation of LMM species are of key concern, this could lead to adverse effects for marine biota in estuaries.

Water-sediment distribution coefficient (K_d), transfer rates for sorption (*k12*) and desorption (*k21*) for Cs as a function of salinity were established in this thesis. The K_d obtained did not reach the state of equilibrium within 1 month. The apparent K_d range was calculated and indicated a decreasing value as a function of increasing salinities, thus Cs is considered conservative (i.e. non-reactive) and is kept in solution.

The transfer rates, both sorption and desorption, were in the same order of magnitude in brackish water with low and high salinity. In general, the sorption rates (*k1*) seemed to decrease by salinity by a factor of two, while the desorption rates (*k2*) were not dependent upon salinity.

The distribution of Cs was, however, dependent upon salinity, thus the time to reach equilibrium conditions will depend upon salinity.

The estimated transfer rates utilized in kinetic models could provide predictions of the dispersal and time dependent distribution of species of Cs in the estuaries of Sandnesfjord, thus providing useful information when performing risk assessments for instance in the event of a release with Cs.

To monitor the distribution of Cs, size-fractionations techniques were utilized. However, to gain information of the degree of fixation of Cs to clay minerals, sequential extractions could be used.

Further investigations regarding the information of the speciation of radionuclides and trace elements are also needed. The speciation is important to incorporate into kinetic transfer models as the speciation will affect the transport of elements in the marine environment. As demonstrated in this thesis, increasing salinity would change the system and hence the distribution of Cs species changed.

8 References

Aldridge, J., Kershaw, P., Brown, J., McCubbin, D., Leonard, K., Young, E., (2003). Transport or plutonium (239/240Pu) and caesium (137Cs) in the Irish Sea: comparison between observations and results from sediment and contaminant transportmodelling. Continental Shelf Research (ISSN: 0278-4343) 23 (9), 869–899. https://doi.org/10.1016/S0278-4343(03)00047-5.

Baranwal V, Ofstad F, Rønning J, Watson R (2011) Mapping of Caesium Fallout from the Chernobyl Accident in the Jotunheimen Area (Report 2011.062). Geological survey of Norway (NGU), Trondheim, Norway

Børretzen, P., Salbu, B., (2002). Fixation of Cs to marine sediments estimated by a stochastic modelling approach. Journal of Environmental Radioactivity (ISSN: 0265-931X) 61 (1), 1–20. https://doi.org/10.1016/S0265-931X(01)00107-2.

Børretzen, P., Salbu, B., (2009). Bioavailability of sediment-associated and low-molecularmass species of radionuclides/trace metals to themussel Mytilus edulis. Journal of Environmental Radioactivity (ISSN: 0265-931X) 100 (4), 333–341. https://doi.org/10.1016/j.jenvrad.2008.12.020

Carvalho, F. P. (2018), Radionuclide concentration processes in marine organisms: A comprehensive review, Journal of Environmental Radioactivity, 186, 124 – 130, doi: 10.1016/j.jenvrad.2017.11.002.

Choi, Y., Kida, S., Takahashi, K., (2013). The impact of oceanic circulation and phase transfer on the dispersion of radionuclides released from the Fukushima Dai-ichi Nuclear Power Plant. Biogeosciences 10 (7), 4911–4925. https://doi.org/10.5194/bg-10-4911-2013.

Choppin, G., Liljenzin, J. O., & Rydberg, J. (2016). Radiochemistry and Nuclear Chemistry: of Nuclear Chemistry, Theory and Applications. Elsevier. p.251, p.285.

Ciffroy, P., Garnier, J. M., & Pham, M. K. (2001). Kinetics of the adsorption and desorption of radionuclides of Co, Mn, Cs, Fe, Ag and Cd in freshwater systems: experimental and modelling approaches. Journal of environmental radioactivity, 55(1), 71-91.

Commission of the European Communities (1998): Atlas of caesium depostion on Europe after the Chernobyl Accident.

Cornell, R. (1993). Adsorption of cesium on minerals: a review. Journal of Radioanalytical and Nuclear Chemistry, 171(2), 483-500.

Devell, L., Tovedal, L., Bergstrøm, U., Applegren, U. et al., (1986). Initial observations of fallout from the reactor accident at Chernobyl. Nature 321, 817-819.

Dietz, L. A., Pachucki, C. F., & Land, G. A. (1963). Half Lives of Cesium-137 and Cesium-134 as Measured by Mass Spectrometry. Analytical Chemistry, 35(7), 797-799.

Duffa, C., du Bois, P.B., Caillaud, M., Charmasson, S., Couvez, C., Didier, D., Dumas, F., Fievet, B., Morillon, M., Renaud, P., Thébault, H., (2016). Development of emergency response tools for accidental radiological contamination of French coastal areas. Journal of Environmental Radioactivity (ISSN: 0265-931X) 151, 487–494. https://doi.org/10.1016/j.jenvrad.2015.04.019.

Evans, D.W., Alberts, J.J., Clark III, R.A., (1983). Reversible ionexchange fixation of cesium-137 leading to mobilization from reservoir sediments. Geochimica et Cosmochimica Acta 47, 1041–1049.

IAEA, (2004). Sediment Distribution Coefficients and Concentration Factors for Biota in the Marine Environment. Technical report series, No. 422International Atomic Energy Agency.

IAEA (2010), Handbook of parameter values for the prediction of radionuclide transfer in terrestrial and freshwater environments, Technical report series, No. 472, International Atomic Energy Agency.

Jaeschke, B. C., Lind, O. C., Bradshaw, C., & Salbu, B. (2015). Retention of radioactive particles and associated effects in the filter-feeding marine mollusc Mytilus edulis. Science of the Total Environment, 502, 1-7.

Karcher, M.J., Gerland, S., Harms, I.H., Iosjpe, M., Heldal, H.E., Kershaw, P.J., Sickel,M., (2004). The dispersion of 99Tc in the Nordic Seas and the Arctic Ocean: a comparison of model results and observations. Journal of Environmental Radioactivity (ISSN: 0265-931X) 74 (1-3), 185–198. https://doi.org/10.1016/j.jenvrad.2004.01.026 Papers from the International Conference on Radioactivity in the Environment, Monaco, 1–5 September 2002.

Kersting, A.B., Efurd, D.W., Finnegan, D.L., Rokop, D.J., Smith, D.K., Thompson, J.L., (1999). Migration of plutonium in ground water at the Nevada Test Site. Nature 397, 56–59. https://doi.org/10.1038/16231.

Kobayashi, T., Otosaka, S., Togawa, O., Hayashi, K., (2007). Development of a

nonconservative radionuclides dispersion model in the ocean and its application to surface cesium-137 dispersion in the Irish Sea. Journal of Nuclear Science and Technology 44 (2), 238–247. https://doi.org/10.1080/18811248.2007.9711278.

Machado, A. A. d. S., K. Spencer, W. Kloas, M. Toffolon, and C. Zarfl (2016), Metal fate and effects in estuaries: A review and conceptual model for better understanding of toxicity, Science of The Total Environment, 541, 268 – 281, doi: https://doi.org/10.1016/j.scitotenv.2015.09.045.

Myers, R. T. (1990). The periodicity of electron affinity. Journal of Chemical Education, 67(4), 307.

Norwegian Environmental Agency (2016): Liming in acidificated Norwegian salmon rivers – Monitoring in 2016. (M-821 | 2017), 31-34.

Norwegian Environmental Agency, Miljøstatus.no (2017): Kadmium og kadmiumforbindelser, retrieved from: https://www.miljostatus.no/tema/kjemikalier/prioritetslisten/kadmium/

Novikov, A.P., Kalmykov, S.N., Utsunomiya, S., Ewing, R.C., Horreard, F., Merkulov, A., Clark, S.B., Tkachev, V.V., Myasoedov, B.F., (2006). Colloid transport of plutonium in the far-field of the Mayak Production Association, Russia. Science (ISSN: 0036-8075) 314 (5799), 638–641. https://doi.org/10.1126/science.1131307.

OECD (1996): Chernobyl Ten Year On. Radiological and Health Impact. An appraisal by the NEA Committee on Radiation Protection and Public Health, November 1995. Paris: OECD, 1996.

Orre, S., Smith, J.N., Alfimov, V., Bentsen, M., (2010). Aprr. Simulating transport of 129I and idealized tracers in the northern North Atlantic Ocean. Environmental Fluid Mechanics (ISSN: 1573-1510) 10 (1), 213–233. https://doi.org/10.1007/s10652-009-9138-3.

Oughton, D. H., Salbu, B., Riise, G., Lien, H., Østby, G. & Nøren, A. (1992). Radionuclide mobility and bioavailability in Norwegian and Soviet soils. Analyst, 117 (3): 481-486.

Oughton, D. H., B_rretzen, P., Salbu, B., & Tronstad, E. (1997). Mobilisation of 137Cs and 90Sr from sediments: Potential sources to arctic waters. The Science of the Total Environment, 202, 155–165.

Periáñez, R., (2005).Modelling the dispersion of radionuclides by a river plume: application to the Rhone River. Continental Shelf Research (ISSN: 0278-4343) 25 (12), 1583–1603. https://doi.org/10.1016/j.csr.2005.04.001.

Periáñez, R., Suh, K. S., & Min, B. I. (2012). Local scale marine modelling of Fukushima releases. Assessment of water and sediment contamination and sensitivity to water circulation description. Marine pollution bulletin, 64(11), 2333-2339.

Periáñez, R., Brovchenko, I., Jung, K., Kim, K., Maderich, V., (2018). The marine K_d and water/sediment interaction problem. Journal of Environmental Radioactivity (ISSN: 0265-931X) 192, 635–647. https://doi.org/10.1016/j.jenvrad.2018.02.014.

Pritchard, D. W., (1967). What is an estuary: physical viewpoint, In Estuaries, American Association for the Advancement of Science, Publication No. 83, Washington, DC..

Rose, D. A. (2005). Lal, R. & Shukla, MK Principles of Soil Physics. Marcel Dekker, New York, 2004. ISBN 0-8247-5324-0. European Journal of Soil Science, 56(5), 683-684. https://doi.org/10.1111/j.1365-2389.2005.0756c.x

Salbu B, Bjornstad HE, Lindstrom NS, Lydersen E, Brevik EM, Rambaek JP, et al. (1985) Size fractionation techniques in the determination of elements associated with particulate or colloidal material in natural fresh waters. Talanta 1985;32:907–13.

Salbu, B. (2000), Speciation of Radionuclides in the Environment, in Encyclopedia of Analytical Chemistry, edited by R. A. Meyers, pp. 12,993–13,016, John Wiley & Sons Ltd, Chichester, https://doi:10.1002/9780470027318.a6308.

Salbu, B. (2000). Source-related characteristics of radioactive particles: a review. Radiation Protection Dosimetry, 92(1-3), 49-54.

Salbu, B., Lind, O. C., & Skipperud, L. (2004). Radionuclide speciation and its relevance in environmental impact assessments. Journal of Environmental Radioactivity, 74(1-3), 233-242.

Salbu, B. (2009), Fractionation of radionuclide species in the environment, Journal of Environmental Radioactivity, 100(4), 283 – 289, https://doi.org/10.1016/j.jenvrad.2008.12.013.

Salbu, B. (2016), Environmental impact and risk assessments and key factors contributing to the overall uncertainties, Journal of Environmental Radioactivity, 151, 352 – 360, https://doi:10.1016/j.jenvrad.2015.09.001.

Sanial, V., K. O. Buesseler, M. A. Charette, and S. Nagao (2017), Unexpected source of Fukushima-derived radiocesium to the coastal ocean of Japan, Proceedings of the National Academy of Sciences, 114(42), 11,092–11,096, doi: https://10.1073/pnas.1708659114.

Strandring, W. J., Oughton, D. H., & Salbu, B. (2002). Potential remobilization of 137Cs, 60Co, 99Tc, and 90Sr from contaminated Mayak sediments in river and estuary environments. Environmental science & technology, 36(11), 2330-2337.

Simonsen, M., Ø. Saetra, P. E. Isachsen, O. C. Lind, H. K. Skjerdal, B. Salbu, H. E. Heldal, and J. P. Gwynn (2017), The impact of tidal and mesoscale eddy advection on the long term dispersion of 99Tc from Sellafield, Journal of Environmental Radioactivity, 177, 100 – 112, https://doi:10.1016/j.jenvrad.2017.06.002.

Simonsen, M, O. C. Lind, Ø. Saetra, P. E. Isachsen, H.-C.. Teien, J. Albretsen, B. Salbu (2019), Coastal transport of river-discharged radionuclides: Impact of speciation and transformation processes in numerical model simulations, Science of the Total Environment, 669, 856–871, https://doi:10.1016/j.scitotenv.2019.01.434

Simonsen, M, H.-C.. Teien, O. C. Lind, Ø. Saetra, J. Albretsen, B. Salbu, (2019) Modeling key processes affecting Al speciation and transport in estuaries, Submitted to Science of the Total Environment.

Skjerdal H, Heldal HE, Gwynn J, Strålberg E, Møller B, Liebig PL, Sværen I, Rand A, Gäfvert T, Haanes H (2017), Radioactivity in the Marine Environment 2012, 2013 and 2014, Results from the Norwegian Marine Monitoring Programme (RAME), Norwegian Radiation Protection Authority.

Skipperud, L., & Salbu, B. (2015). Sequential extraction as a tool for mobility studies of radionuclides and metals in soils and sediments. Radiochimica Acta, 103(3), 187-197.

Skipperud L, Oughton D, Salbu B., (2000). The impact of Pu speciation on distribution coefficients in Mayak soil. Science of the Total Environment; 257: 81-93

Skipperud L, Oughton DH, Salbu B., (2000) The impact of plutonium speciation on the distribution coefficients in a sediment-sea water system, and radiological assessment of doses to humans. Health Physics; 79: 147-153.

Skuterud L, Thørring H, Ytre-Eide MA (2014) Use of total 137Cs deposition to predict contamination in feed vegetation and reindeer 25 years after Chernobyl. Paper presented at the ICRER 2014 Third International Conference on Radioecology and Environmental Radioactivity, Barcelona, Spain

Smith, C., Goshawk, J., Charles, K., McDonald, P., Leonard, K., McCubbin, D., (2003). MEAD (part II)—predictions of radioactivity concentrations in the Irish Sea. Journal of Environmental Radioactivity (ISSN: 0265-931X) 68 (3), 193–214. https://doi.org/10.1016/S0265-931X(03)00041-9.

Stuanes, A.O., (1998), Norges Landbrukshøgskole.

Teien, H.-C.,W. J. Standring, and B. Salbu (2006), Mobilization of river transported colloidal aluminium upon mixing with seawater and subsequent deposition in fish gills, Science of The Total Environment, 364(1), 149 – 164, https://doi.org/10.1016/j.scitotenv.2006.01.005.

Tsumune, D., Tsubono, T., Aoyama, M., Uematsu, M., Misumi, K., Maeda, Y., Yoshida, Y., Hayami, H., (2013). One-year, regional-scale simulation of 137Cs radioactivity in the ocean following the Fukushima Dai-ichi Nuclear Power Plant accident. Biogeosciences 10 (8), 5601–5617. https://doi.org/10.5194/bg-10-5601-2013.

UNSCEAR (2000), Sources and effects of ionizing radiation: sources, vol. 1, United Nations Publications, United Nations. Scientific Committee on the Effects of Atomic Radiation.

VanLonn, G. W, Duffy, S.J (2011), environmental chemistry, a global perspective.

Third edition. Oxford press, 317-340.

Vives i Batlle, J., Aoyama,M., Bradshaw, C., Brown, J., Buesseler, K., Casacuberta, N., Christl, M., Duffa, C., Impens, N., Iosjpe,M., MasquÃl', P., Nishikawa, J., (2018). Marine radioecology after the Fukushima Dai-ichi nuclear accident: are we better positioned to understand the impact of radionuclides in marine ecosystems? Science of The Total Environment (ISSN: 0048-9697) 618 (Supplement C), 80–92. https://doi.org/10.1016/j.scitotenv.2017.11.005.

Ytre-Eide, M. A., W. J. Standring, I. Amundsen, M. Sickel, A. Liland, J. Saltbones, J. Bartnicki, H. Haakenstad, and B. Salbu (2009), Consequences in Norway of a hypothetical accident at Sellafield: Potential release–transport and fallout, Tech. Rep. StrålevernRapport2009: 7, Statens Straalevern.

9 Appendix

1. Appendix A - Experimental weights clay
2. Appendix B – Experimental weights collloids
3. Appendix C – Activity in clay
4. Appendix D – Activity in colloids
5. Appendix E – Clay content
6. Appendix F - Distribution coefficient, K_d
7. Appendix G - Determination of transformation rates

9.1 Appendix A - Experimental weights clay

Table A1 – A6: Remobilization of ^{134}Cs and sorption of ^{137}Cs from/to clay fraction. Experimental weights for each fraction, LMM, HMM and >0.45μm. The weight for total amount and LMM fraction determined by analytical balance with accuracy 0.0001 g. The weight of both HMM and clay calculated. Extraction times 0.5h, 2h, 5h, 24h, 8 days and 1 month.

Extraction time 0,5 hours **Sample – *PSU* value**	**Total amount (g) in centrifuge tube before centrifuge**	**Amount (g) in LMM fraction**	***Calculated weight for HMM (g)*** **Difference before and after centrifuge (total - LMM)**	**Calculated weight for clay (g) (>0,45 um)** **(Total amount * clay gr/ml)**
1-1	7,8547	7,4626	0,3921	0,05341196
1-2	7,9617	7,5121	0,4496	0,05413956
1-3	7,8512	7,4699	0,3813	0,05338816
3-1	8,0147	7,6364	0,3783	0,05449996
3-2	7,9917	7,5857	0,406	0,05434356
3-3	7,9901	7,6402	0,3499	0,05433268
5-1	7,9807	7,6186	0,3621	0,05426876
5-2	8,1795	7,8225	0,357	0,0556206
5-3	8,2348	7,8881	0,3467	0,05599664
10-1	8,0386	7,6554	0,3832	0,05466248
10-2	7,979	7,5061	0,4729	0,0542572
10-3	8,0947	7,6645	0,4302	0,05504396
15-1	8,0164	7,5979	0,4185	0,05451152
15-2	8,0961	7,6706	0,4255	0,05505348
15-3	8,0276	7,5305	0,4971	0,05458768
25-1	8,0566	7,6141	0,4425	0,05478488
25-2	8,1059	7,6518	0,4541	0,05512012
25-3	8,1243	7,671	0,4533	0,05524524
B-1	7,9562	7,5269	-	-
B-2	7,7116	7,3068	-	-
B-3	7,7505	7,3484	-	-

Table A2

Extraction time 2 hours **Sample – *PSU* value**	**Total amount (g) in centrifuge tube before centrifuge**	**Amount (g) in LMM fraction**	***Calculated weight for HMM (g)*** **Difference before and after centrifuge (total - LMM)**	**Calculated weight for clay (g) (>0,45 um)** **(Total amount * clay gr/ml)**
1-1	8,1908	7,75	0,4408	0,05569744
1-2	8,0362	7,6442	0,392	0,05464616
1-3	7,9424	7,5709	0,3715	0,05400832
3-1	8,073	7,702	0,371	0,0548964
3-2	7,8465	7,4374	0,4091	0,0533562
3-3	7,8846	7,4929	0,3917	0,05361528
5-1	8,0498	7,624	0,4258	0,05473864
5-2	7,8765	7,491	0,3855	0,0535602
5-3	7,8894	7,417	0,4724	0,05364792
10-1	8,0544	7,6374	0,417	0,05476992
10-2	8,1217	7,6512	0,4705	0,05522756
10-3	8,0387	7,5979	0,4408	0,05466316
15-1	8,2311	7,7911	0,44	0,05597148
15-2	7,9443	7,4549	0,4894	0,05402124
15-3	8,059	7,5785	0,4805	0,0548012
25-1	7,984	7,4844	0,4996	0,0542912
25-2	8,0668	7,6113	0,4555	0,05485424
25-3	8,0905	7,5976	0,4929	0,0550154
B-1	7,866	7,5923	-	-
B-2	7,7115	7,4199	-	-
B-3	8,0629	7,7938	-	-

Table A3

Extraction 5 hours **Sample – *PSU* value**	**Total amount (g) in centrifuge tube before centrifuge**	**Amount (g) in LMM fraction**	***Calculated weight for HMM (g)*** **Difference before and after centrifuge (total - LMM)**	**Calculated weight for clay (g) (>0,45 um)** **(Total amount * clay gr/ml)**
1-1	7,9897	7,5783	0,4114	0,05432996
1-2	7,9764	7,5382	0,4382	0,05423952
1-3	7,9632	7,538	0,4252	0,05414976
3-1	7,9686	7,4444	0,5242	0,05418648
3-2	7,8925	7,4762	0,4163	0,053669
3-3	8,1967	7,7581	0,4386	0,05573756
5-1	8,2437	7,7603	0,4834	0,05605716
5-2	8,2802	7,8938	0,3864	0,05630536
5-3	7,9845	7,6343	0,3502	0,0542946
10-1	8,0772	7,6327	0,4445	0,05492496
10-2	7,9302	7,5539	0,3763	0,05392536
10-3	8,1086	7,1314	0,9772	0,05513848
15-1	8,3753	7,9086	0,4667	0,05695204
15-2	8,0428	7,6115	0,4313	0,05469104
15-3	8,0024	7,5512	0,4512	0,05441632
25-1	8,3068	7,8651	0,4417	0,05648624
25-2	8,2573	7,848	0,4093	0,05614964
25-3	8,1684	7,6846	0,4838	0,05554512
B-1	8,0148	7,628	-	-
B-2	7,839	7,4328	-	-
B-3	7,8782	7,5204	-	-

Table A4

Extraction 24 hours **Sample – *PSU* value**	**Total amount (g) in centrifuge tube before centrifuge**	**Amount (g) in LMM fraction**	***Calculated weight for HMM (g)*** **Difference before and after centrifuge (total - LMM)**	**Calculated weight for clay (g) (>0,45 um)** **(Total amount * clay gr/ml)**
1-1	8,0587	7,6763	0,3824	0,05479916
1-2	7,8972	7,4461	0,4511	0,05370096
1-3	8,027	7,5959	0,4311	0,0545836
3-1	7,996	7,4384	0,5576	0,0543728
3-2	7,826	7,2919	0,5341	0,0532168
3-3	7,9701	7,4749	0,4952	0,05419668
5-1	8,1333	7,6828	0,4505	0,05530644
5-2	7,823	6,871	0,952	0,0531964
5-3	7,8542	7,4345	0,4197	0,05340856
10-1	7,8429	7,2499	0,593	0,05333172
10-2	7,7784	7,2508	0,5276	0,05289312
10-3	8,0115	7,49	0,5215	0,0544782
15-1	7,4515	6,9344	0,5171	0,0506702
15-2	7,9689	7,509	0,4599	0,05418852
15-3	7,9645	7,4351	0,5294	0,0541586
25-1	7,8456	7,3329	0,5127	0,05335008
25-2	7,9206	7,4322	0,4884	0,05386008
25-3	8,1938	7,6134	0,5804	0,05571784
B-1	7,9154	7,642	-	-
B-2	7,5978	7,319	-	-
B-3	7,7584	7,4484	-	-

Table A5

Extraction 8 days **Sample – *PSU* value**	**Total amount (g) in centrifuge tube before centrifuge**	**Amount (g) in LMM fraction**	***Calculated weight for HMM (g)*** **Difference before and after centrifuge (total - LMM)**	**Calculated weight for clay (g) (>0,45 um)** **(Total amount * clay gr/ml)**
1-1	8,17	7,7122	0,4578	0,055556
1-2	7,72	7,327	0,393	0,052496
1-3	8,38	7,9712	0,4088	0,056984
3-1	8,43	8,0092	0,4208	0,057324
3-2	7,97	7,5325	0,4375	0,054196
3-3	8,18	7,3638	0,8162	0,055624
5-1	8,32	7,8967	0,4233	0,056576
5-2	7,83	7,3614	0,4686	0,053244
5-3	8,13	7,7072	0,4228	0,055284
10-1	8,2	7,7685	0,4315	0,05576
10-2	7,95	7,5283	0,4217	0,05406
10-3	8,16	7,7836	0,3764	0,055488
15-1	8,13	7,7286	0,4014	0,055284
15-2	7,97	7,5611	0,4089	0,054196
15-3	8,24	7,7051	0,5349	0,056032
25-1	8,15	7,7348	0,4152	0,05542
25-2	8,07	7,6473	0,4227	0,054876
25-3	8,4	7,8969	0,5031	0,05712
B-1	7,9	7,4517	-	-
B-2	8,3	7,8786	-	-
B-3	7,79	7,4132	-	-

Table A6

Extraction 1 month **Sample – *PSU* value**	**Total amount (g) in centrifuge tube before centrifuge**	**Amount (g) in LMM fraction**	***Calculated weight for HMM (g)*** **Difference before and after centrifuge (total - LMM)**	**Calculated weight for clay (g) (>0,45 um)** **(Total amount * clay gr/ml)**
1-1	7,0117	6,1986	0,8131	0,04767956
1-2	7,3792	6,6633	0,7159	0,05017856
1-3	8,1211	7,3835	0,7376	0,05522348
3-1	7,18	6,3574	0,8226	0,048824
3-2	8,13	7,3583	0,7717	0,055284
3-3	7,778	7,0644	0,7136	0,0528904
5-1	7,5437	6,662	0,8817	0,05129716
5-2	7,86	7,1366	0,7234	0,053448
5-3	7,6	6,872	0,728	0,05168
10-1	7,999	7,039	0,96	0,0543932
10-2	8,006	7,1838	0,8222	0,0544408
10-3	8,052	7,1002	0,9518	0,0547536
15-1	8,03	7,3311	0,6989	0,054604
15-2	7,879	7,0431	0,8359	0,0535772
15-3	7,9679	7,0567	0,9112	0,05418172
25-1	8,31	7,3801	0,9299	0,056508
25-2	8,17	7,7638	0,4062	0,055556
25-3	7,78	6,8481	0,9319	0,052904
B-1	7,95	7,1952	-	-
B-2	7,56	6,679	-	-
B-3	7,83	6,9186	-	-

9.2 Appendix B – Experimental weights colloids

Table B1 – B6: Remobilization of ^{134}Cs and sorption of ^{137}Cs from/to colloidal fraction. Experimental weights for each fraction, LMM, HMM. The weight for total amount and LMM fraction determined by analytical balance with accuracy 0.0001 g. The weight of HMM calculated. Extraction times 0.5h, 2h, 5h, 24h, 8 days and 1 month.

Extraction time 0,5 hours **Sample – *PSU* value**	**Total amount (g) in centrifuge tube before centrifuge**	**Amount (g) in LMM fraction**	***Calculated weight for HMM (g)*** **Difference before and after centrifuge (total - LMM)**
1-1	8,0696	7,6968	0,3728
1-2	8,0916	7,6739	0,4177
1-3	8,0923	7,6945	0,3978
3-1	8,1882	7,6609	0,5273
3-2	8,0694	7,6465	0,4229
3-3	8,2835	7,9127	0,3708
5-1	8,0334	7,5788	0,4546
5-2	8,1769	7,7625	0,4144
5-3	8,0536	7,663	0,3906
10-1	8,0665	7,6611	0,4054
10-2	8,0067	7,6292	0,3775
10-3	7,9626	7,4913	0,4713
15-1	8,0794	7,6042	0,4752
15-2	8,1629	7,6277	0,5352
15-3	8,1336	7,6754	0,4582
25-1	7,9362	7,4649	0,4713
25-2	8,2143	7,7081	0,5062
25-3	8,0877	7,5528	0,5349

Table B2

Extraction time 2 hours **Sample – *PSU* value**	**Total amount (g) in centrifuge tube before centrifuge**	**Amount (g) in LMM fraction**	***Calculated weight for HMM (g)*** **Difference before and after centrifuge (total - LMM)**
1-1	7,9698	7,5425	0,4273
1-2	8,0907	7,6818	0,4089
1-3	8,197	7,8012	0,3958
3-1	8,14	7,7301	0,4099
3-2	8,1162	7,6955	0,4207
3-3	7,8672	7,5058	0,3614
5-1	8,4158	8,0062	0,4096
5-2	8,1588	7,7928	0,366
5-3	8,0645	7,6455	0,419
10-1	8,3165	7,9016	0,4149
10-2	8,4434	8,0227	0,4207
10-3	8,1979	7,8387	0,3592
15-1	8,07	7,6144	0,4556
15-2	8,29	7,8465	0,4435
15-3	7,96	7,443	0,517
25-1	7,94	7,4855	0,4545
25-2	8,25	7,847	0,403
25-3	8,54	8,053	0,487

Table B3

Extraction time 5 hours **Sample – *PSU* value**	**Total amount (g) in centrifuge tube before centrifuge**	**Amount (g) in LMM fraction**	***Calculated weight for HMM (g)*** **Difference before and after centrifuge (total - LMM)**
1-1	8,12	7,5193	0,6007
1-2	7,97	7,6341	0,3359
1-3	7,77	7,3888	0,3812
3-1	7,89	7,5231	0,3669
3-2	7,85	7,4435	0,4065
3-3	7,85	7,4897	0,3603
5-1	7,86	7,4306	0,4294
5-2	7,87	7,4519	0,4181
5-3	7,96	7,4865	0,4735
10-1	7,96	7,5501	0,4099
10-2	8,18	7,7742	0,4058
10-3	8,01	7,604	0,406
15-1	8,06	7,605	0,455
15-2	7,98	7,5974	0,3826
15-3	8,01	7,6231	0,3869
25-1	8,33	7,8728	0,4572
25-2	8,14	7,7069	0,4331
25-3	8,19	7,7115	0,4785

Table B4

Extraction time 24 hours **Sample – *PSU* value**	**Total amount (g) in centrifuge tube before centrifuge**	**Amount (g) in LMM fraction**	***Calculated weight for HMM (g)*** **Difference before and after centrifuge (total - LMM)**
1-1	7,79	7,398	0,392
1-2	7,89	7,5272	0,3628
1-3	8,12	7,7116	0,4084
3-1	8,05	7,631	0,419
3-2	7,97	7,5795	0,3905
3-3	7,86	7,4244	0,4356
5-1	7,94	7,5346	0,4054
5-2	8,01	7,6028	0,4072
5-3	7,93	7,5376	0,3924
10-1	7,91	7,4666	0,4434
10-2	8,13	7,7184	0,4116
10-3	7,91	7,5445	0,3655
15-1	7,97	7,5639	0,4061
15-2	8,1	7,222	0,878
15-3	8,08	7,6868	0,3932
25-1	8,01	7,5745	0,4355
25-2	8,04	7,5799	0,4601
25-3	8,16	7,7575	0,4025

Table B5

Extraction time 8 days **Sample – *PSU* value**	**Total amount (g) in centrifuge tube before centrifuge**	**Amount (g) in LMM fraction**	***Calculated weight for HMM (g)*** **Difference before and after centrifuge (total - LMM)**
1-1	8,16	7,761	0,399
1-2	8,1	7,7013	0,3987
1-3	7,95	7,5916	0,3584
3-1	8,12	7,6722	0,4478
3-2	7,9	7,484	0,416
3-3	7,98	7,581	0,399
5-1	7,94	7,5732	0,3668
5-2	8,1	7,6813	0,4187
5-3	8,09	7,7594	0,3306
10-1	7,95	7,4995	0,4505
10-2	8,07	7,6417	0,4283
10-3	8,26	7,8125	0,4475
15-1	8,05	7,5804	0,4696
15-2	8,17	7,7718	0,3982
15-3	8,01	7,6008	0,4092
25-1	8,35	7,7708	0,5792
25-2	8,34	7,8951	0,4449
25-3	8,28	7,8192	0,4608

Table B6

Extraction time 1 month **Sample – *PSU* value**	**Total amount (g) in centrifuge tube before centrifuge**	**Amount (g) in LMM fraction**	***Calculated weight for HMM (g)*** **Difference before and after centrifuge (total - LMM)**
1-1	7,65	6,9499	0,7001
1-2	7,67	7,053	0,617
1-3	8,15	7,5088	0,6412
3-1	7,97	7,3223	0,6477
3-2	8,03	7,3791	0,6509
3-3	7,99	7,2524	0,7376
5-1	7,97	7,2769	0,6931
5-2	7,97	7,3489	0,6211
5-3	7,94	7,3057	0,6343
10-1	8,11	7,4583	0,6517
10-2	7,97	7,2772	0,6928
10-3	8,2	7,5999	0,6001
15-1	8,08	7,2751	0,8049
15-2	8,13	7,4065	0,7235
15-3	8,16	7,426	0,734
25-1	8,19	7,4456	0,7444
25-2	7,99	7,204	0,786
25-3	8,08	7,2955	0,7845

9.3 Appendix C – Activity in clay

Table C1 – C6 The DPM (disintegration per minute) and percentage distribution of LMM, HMM and >0.45 μm for the remobilization of ^{134}Cs and the sorption of ^{137}Cs from/to clay. DPM calculated by equation 4. The efficiency of ^{134}Cs and ^{137}Cs was 0.2 and 0.17 respectively.

Extraction time 0,5 hours	**134Cs**						**137Cs**					
	DPM			**Percentage distribution**			**DPM**			**Percentage distribution**		
Sample – *PSU* value	**DPM LMM**	**DPM HMM**	**DPM >0.45 μm**	**% distribution LMM**	**% distribution HMM***	**% distribution >0.45 μm**	**DPM LMM**	**DPM HMM**	**DPM >0.45 μm**	**% distribution LMM**	**% distribution HMM***	**% distribution >0.45 μm**
1-1	105,3	-28,4	569,5	16	0	84	644,4	0,9	107,8	86	0	14
1-2	101,6	37,1	574,9	14	5	81	581,9	-0,3	164,4	78	0	22
1-3	133,3	6,5	566,9	19	1	80	619,4	1,0	147,7	81	0	19
3-1	149,8	16,7	522,5	22	2	76	619,0	0,8	160,2	79	0	21
3-2	176,4	-20,2	505,3	26	0	74	677,1	0,3	93,6	88	0	12
3-3	177,8	-6,5	560,2	24	0	76	683,5	1,5	135,4	83	0	17
5-1	137,5	3,3	514,7	21	0	79	676,1	0,7	96,5	87	0	12
5-2	189,3	-3,3	534,5	26	0	74	709,3	2,0	79,5	90	0	10
5-3	215,8	23,6	594,7	26	3	71	704,5	0,2	69,8	91	0	9
10-1	153,5	2,4	527,1	22	0	77	723,3	5,7	63,1	91	0	8
10-2	253,3	19,5	494,4	33	3	64	638,5	1,2	52,8	92	0	8
10-3	158,2	9,6	474,7	25	1	74	729,8	1,1	67,9	91	0	9
15-1	226,2	-12,7	553,6	29	0	71	725,6	0,4	45,8	94	0	6
15-2	204,0	-15,6	447,8	31	0	69	708,3	-0,1	45,1	94	0	6
15-3	208,2	3,6	479,8	30	1	69	714,9	0,6	38,8	95	0	5
25-1	153,3	0,9	561,5	21	0	78	718,1	1,1	33,6	95	0	4
25-2	240,0	15,1	530,7	31	2	68	721,5	1,1	43,6	94	0	6
25-3	179,8	30,0	516,9	25	4	71	733,6	0,3	40,1	95	0	5

*negative values set to zero for the calculation of percentage distribution.

Table C1:

Extraction time 2 hours	^{134}Cs						^{137}Cs					
	DPM			Percentage distribution			DPM			Percentage distribution		
Sample – *PSU* value	DPM LMM	DPM HMM*	DPM >0.45 *µm*	% distribution LMM	% distribution HMM	% distribution >0.45 *µm*	DPM LMM	DPM HMM	DPM >0.45 *µm*	% distribution LMM	% distribution HMM	% distribution >0.45 *µm*
1-1	155,1	-3,5	503,8	24	0	76	566,9	1,4	192,6	75	0	25
1-2	180,5	-20,4	554,0	25	0	75	600,2	1,1	174,7	77	0	23
1-3	191,8	-5,3	490,9	28	0	72	548,3	1,1	179,6	75	0	25
3-1	202,4	-0,4	557,6	27	0	73	622,0	1,3	118,6	84	0	16
3-2	213,5	-16,7	424,2	33	0	67	671,0	0,6	126,3	84	0	16
3-3	169,3	-14,9	500,0	25	0	75	632,3	0,9	127,3	83	0	17
5-1	205,1	10,4	517,1	28	0	71	658,8	1,7	118,2	85	0	15
5-2	199,3	-36,2	487,5	29	0	71	659,4	2,3	98,6	87	0	13
5-3	220,2	3,3	492,0	31	0	69	655,9	-0,2	104,9	86	0	14
10-1	228,0	16,2	455,6	33	0	65	667,7	0,5	78,1	89	0	10
10-2	231,5	2,2	483,5	32	0	67	664,6	1,0	70,4	90	0	10
10-3	267,6	26,9	463,5	35	0	61	710,9	1,7	85,8	89	0	11
15-1	251,1	4,5	484,4	34	0	65	714,2	0,4	48,3	94	0	6
15-2	212,9	22,2	504,0	29	0	68	687,9	0,6	54,8	93	0	7
15-3	241,8	8,2	462,2	34	0	65	690,1	1,3	70,3	91	0	9
25-1	221,8	-22,7	544,9	29	0	71	679,7	0,8	48,6	93	0	7
25-2	227,3	-16,0	524,0	30	0	70	717,2	1,1	44,8	94	0	6
25-3	235,3	27,8	458,0	33	0	64	717,9	1,7	58,6	92	0	8

*negative values set to zero for the calculation of percentage distribution.

Table C2:

Extraction time 5 hours	^{134}Cs						^{137}Cs					
	DPM			Percentage distribution			DPM			Percentage distribution		
Sample – *PSU* value	DPM LMM	DPM HMM	DPM >0.45 *µm*	% distribution LMM	% distribution HMM*	% distribution >0.45 *µm*	DPM LMM	DPM HMM	DPM >0.45 *µm*	% distribution LMM	% distribution HMM	% distribution >0.45 *µm*
1-1	199,6	14,9	450,4	30	2	68	529,1	0,0	231,1	70	0	30
1-2	224,7	18,9	450,7	32	3	65	546,8	0,7	241,6	69	0	31
1-3	178,0	4,4	516,9	25	1	74	532,0	1,7	226,3	70	0	30
3-1	235,8	1,8	518,7	31	0	69	620,7	0,3	158,4	80	0	20
3-2	250,4	2,7	451,6	36	0	64	604,6	1,3	167,3	78	0	22
3-3	262,0	-11,6	468,9	36	0	64	634,5	1,0	179,7	78	0	22
5-1	269,3	24,9	414,2	38	4	58	629,2	0,7	113,9	85	0	15
5-2	248,4	18,5	415,1	36	3	61	663,7	1,3	121,6	84	0	16
5-3	271,3	10,9	502,4	35	1	64	639,3	1,8	115,8	85	0	15
10-1	284,9	10,5	403,1	41	1	58	724,5	1,8	57,4	93	0	7
10-2	287,8	-25,6	435,5	40	0	60	659,9	2,2	103,4	86	0	14
10-3	328,9	-11,1	470,9	41	0	59	681,2	0,8	88,8	88	0	12
15-1	277,8	8,9	492,7	36	1	63	735,3	1,1	79,6	90	0	10
15-2	218,9	25,1	496,0	30	3	67	729,8	1,2	73,9	91	0	9
15-3	262,0	10,2	462,9	36	1	63	705,6	1,2	68,2	91	0	9
25-1	305,3	16,5	506,4	37	2	61	720,9	1,2	65,3	92	0	8
25-2	283,3	-4,9	486,0	37	0	63	717,6	1,1	47,3	94	0	6
25-3	304,0	-0,7	445,3	41	0	59	726,6	0,1	47,3	94	0	6

*negative values set to zero for the calculation of percentage distribution.

Table C3:

Extraction time 24 hours	^{134}Cs						^{137}Cs					
	DPM			Percentage distribution			DPM			Percentage distribution		
Sample – *PSU* value	DPM LMM	DPM HMM	DPM >0.45 *µm*	% distribu-ion LMM	% distribution HMM	% distribu-ion >0.45 *µm*	DPM LMM	DPM HMM	DPM >0.45 *µm*	% distribu-ion LMM	% distribution HMM	% distribu-ion >0.45 *µm*
1-1	246,9	12,5	354,0	40	2	58	502,8	1,1	208,0	71	0	29
1-2	252,7	1,8	422,5	37	0	63	463,8	-0,3	263,9	64	0	36
1-3	268,0	39,8	431,1	36	5	58	475,9	0,2	312,7	60	0	40
3-1	261,5	9,3	399,3	39	1	60	528,7	0,9	219,1	71	0	29
3-2	220,2	6,2	397,1	35	1	64	561,0	0,5	224,7	71	0	29
3-3	268,9	18,7	340,0	43	3	54	547,3	-0,1	177,7	75	0	25
5-1	275,5	16,2	411,6	39	2	59	586,8	0,9	184,1	76	0	24
5-2	234,9	22,7	387,6	36	4	60	564,0	1,0	161,3	78	0	22
5-3	332,4	-28,2	461,8	43	0	60	549,7	0,4	174,9	76	0	24
10-1	268,0	14,5	335,1	43	2	54	625,3	1,1	113,7	85	0	15
10-2	271,5	-1,6	353,3	44	0	57	615,9	0,6	102,8	86	0	14
10-3	322,7	4,7	459,5	41	1	58	627,0	1,1	119,4	84	0	16
15-1	282,7	-14,4	332,2	47	0	55	629,7	1,3	72,5	90	0	10
15-2	354,5	1,1	406,7	47	0	53	665,2	1,3	96,3	87	0	13
15-3	271,8	11,8	396,4	40	2	58	645,8	0,7	99,9	87	0	13
25-1	331,8	42,2	392,5	43	6	51	671,1	-0,1	78,3	90	0	10
25-2	330,4	14,5	383,1	45	2	53	686,8	0,0	61,9	92	0	8
25-3	361,1	-22,4	381,5	50	0	53	704,4	1,5	74,7	90	0	10

*negative values set to zero for the calculation of percentage distribution.

Table C4:

Extraction time 8 days	134Cs						137Cs					
	DPM			Percentage distribution			DPM			Percentage distribution		
Sample – *PSU* value	DPM LMM	DPM HMM	DPM >0.45 *µm*	% distribution LMM	% distribution HMM	% distribution >0.45 *µm*	DPM LMM	DPM HMM	DPM >0.45 *µm*	% distribution LMM	% distribution HMM	% distribution >0.45 *µm*
1-1	261,5	9,3	422,0	38	1	61	406,0	5,0	383,1	51	1	48
1-2	245,3	-0,7	377,5	39	0	61	371,7	5,8	313,0	54	1	45
1-3	245,3	4,7	423,6	36	1	63	412,4	6,0	404,8	50	1	49
3-1	293,3	2,9	390,0	43	0	57	486,8	-0,1	301,5	62	0	38
3-2	282,5	2,2	388,5	42	0	58	471,0	12,1	310,9	59	2	39
3-3	266,5	27,6	376,9	40	4	56	473,3	7,5	311,4	60	1	39
5-1	326,9	-23,8	366,7	47	0	53	509,9	5,6	261,9	65	1	34
5-2	235,8	17,1	336,7	40	3	57	488,6	2,4	237,9	67	0	33
5-3	326,9	2,9	398,5	45	0	55	487,1	6,8	244,6	66	1	33
10-1	346,2	10,0	352,0	49	1	50	586,6	7,1	151,8	79	1	20
10-2	380,9	26,7	359,6	50	3	47	552,3	4,5	159,6	77	1	22
10-3	335,3	14,9	364,9	47	2	51	593,9	0,6	171,6	78	0	22
15-1	370,0	3,3	380,2	49	0	51	616,3	1,9	131,0	82	0	18
15-2	342,7	-16,4	303,6	53	0	47	620,3	3,8	122,4	83	1	16
15-3	278,9	-0,7	372,7	43	0	57	639,8	4,8	138,5	82	0	18
25-1	414,0	17,5	387,5	51	2	47	653,2	4,2	102,6	86	1	13
25-2	343,6	-20,4	383,1	47	0	53	687,1	12,2	91,4	87	1	12
25-3	413,6	-5,1	329,3	56	0	44	713,0	8,6	80,1	89	1	10

*negative values set to zero for the calculation of percentage distribution.

Table C5:

Extraction time 1 month	134Cs						137Cs					
	DPM			Percentage distribution			DPM			Percentage distribution		
Sample – *PSU* value	DPM LMM	DPM HMM	DPM >0.45 *µm*	% distribution LMM	% distribution HMM	% distribution >0.45 *µm*	DPM LMM	DPM HMM	DPM >0.45 *µm*	% distribution LMM	% distribution HMM	% distribution >0.45 *µm*
1-1	189,6	13,8	26,0	83	6	11	251,8	3,1	46,4	84	1	15
1-2	196,4	0,0	340,9	37	0	63	291,7	6,1	344,1	45	1	54
1-3	255,5	13,3	160,5	60	3	37	322,5	-1,8	152,1	68	0	32
3-1	239,8	-6,7	199,5	55	0	45	351,2	6,3	194,3	64	1	35
3-2	239,3	-6,9	320,9	43	0	57	417,8	5,5	309,3	57	1	42
3-3	243,6	-2,2	292,5	45	0	55	398,8	7,1	238,5	62	1	37
5-1	264,2	2,7	234,9	53	0	47	397,4	10,6	227,9	62	2	36
5-2	267,6	20,0	318,0	44	3	53	439,4	-1,1	248,3	64	0	36
5-3	305,1	-16,5	401,3	43	0	57	407,6	0,4	269,4	60	0	40
10-1	312,7	6,4	341,5	47	1	52	485,9	6,8	209,3	69	1	30
10-2	334,9	4,5	237,8	58	1	41	484,9	1,9	165,1	75	0	25
10-3	340,9	47,1	233,1	55	8	37	500,4	3,4	151,5	76	1	23
15-1	325,6	1,1	285,6	53	0	47	576,1	7,7	141,9	79	1	20
15-2	362,7	1,1	211,3	63	0	37	572,8	6,3	111,3	83	1	16
15-3	290,2	-8,0	236,5	55	0	45	560,1	18,8	123,2	80	2	18
25-1	369,3	20,9	164,7	66	4	30	610,6	11,3	38,1	92	2	6
25-2	338,0	7,6	226,7	59	1	40	637,8	11,0	96,1	86	1	13
25-3	309,5	32,5	166,7	61	6	33	584,8	1,0	47,3	92	0	8

*negative values set to zero for the calculation of percentage distribution.

9.4 Annex D: Activity in colloids

Table D1 – D6: The DPM (disintegration per minute) and percentage distribution of LMM, HMM and >0.45 *µm* for the remobilization of ^{134}Cs and the sorption of ^{137}Cs from/to clay. DPM calculated by equation 4. The efficiency of ^{134}Cs and ^{137}Cs was 0.2 and 0.17 respectively.

Extraction time 0,5 hours	**^{134}Cs**						**^{137}Cs**					
	DPM			**Percentage distribution**			**DPM**			**Percentage distribution**		
Sample – *PSU* value	**DPM LMM**	**DPM HMM**	**DPM >0.45 *µm***	**% distribution LMM**	**% distribution HMM***	**% distribution >0.45 *µm***	**DPM LMM**	**DPM HMM**	**DPM >0.45 *µm***	**% distribution LMM**	**% distribution HMM***	**% distribution >0.45 *µm***
1-1	489,1	-15,8		100	0		740,4	1,4		100	0	
1-2	426,7	-16,0		100	0		796,2	-2,4		100	0	
1-3	399,6	-21,1		100	0		775,4	-0,7		100	0	
3-1	341,6	-42,9		100	0		779,9	-0,3		100	0	
3-2	429,5	6,4		99	1		728,2	-6,2		100	0	
3-3	412,0	-25,1		100	0		799,9	1,8		100	0	
5-1	413,3	-0,9		100	0		744,2	-1,3		100	0	
5-2	416,9	15,5		96	4		766,3	-1,6		100	0	
5-3	397,3	8,7		98	2		694,2	3,9		99	1	
10-1	422,7	-11,5		100	0		765,6	0,9		100	0	
10-2	438,0	-28,4		100	0		754,9	3,3		100	0	
10-3	391,5	15,1		96	4		737,8	7,1		99	1	
15-1	405,5	8,2		98	2		765,9	-6,6		100	0	
15-2	456,5	16,7		96	4		703,4	-2,8		100	0	
15-3	393,3	-18,0		100	0		728,7	4,9		99	1	
25-1	457,3	-9,1		100	0		728,7	-13,7		100	0	
25-2	462,4	-0,5		100	0		738,8	1,5		100	0	
25-3	406,2	-21,5		100	0		735,4	-8,1		100	0	

*negative values set to zero for the calculation of percentage distribution.

Table D2:

Extraction time 2 hours	^{134}Cs						^{137}Cs					
	DPM			Percentage distribution			DPM			Percentage distribution		
Sample – *PSU* value	DPM LMM	DPM HMM	DPM >0.45 *µm*	% distribution LMM	% distribution HMM*	% distribution >0.45 *µm*	DPM LMM	DPM HMM	DPM >0.45 *µm*	% distribution LMM	% distribution HMM*	% distribution >0.45 *µm*
1-1	406,7	0,0		100	0		726,6	0,0		100	0	
1-2	414,9	0,0		100	0		767,4	0,0		100	0	
1-3	453,6	1,5		100	0		775,9	0,0		100	0	
3-1	311,1	0,0		100	0		765,9	0,0		100	0	
3-2	436,5	0,0		100	0		759,6	0,0		100	0	
3-3	341,5	0,0		100	0		766,6	0,0		100	0	
5-1	410,5	3,8		99	1		765,6	0,0		100	0	
5-2	423,1	0,0		100	0		764,3	0,0		100	0	
5-3	449,3	3,8		99	1		682,6	0,0		100	0	
10-1	418,9	0,0		100	0		780,4	0,0		100	0	
10-2	460,9	0,0		100	0		783,8	1,0		100	0	
10-3	428,4	0,0		100	0		788,6	0,0		100	0	
15-1	398,0	0,0		100	0		742,7	6,1		99	1	
15-2	436,9	7,1		98	2		793,9	0,0		100	0	
15-3	365,1	0,0		100	0		722,6	0,0		100	0	
25-1	429,5	0,0		100	0		714,6	0,0		100	0	
25-2	491,6	0,0		100	0		710,1	2,9		100	0	
25-3	496,9	0,0		100	0		757,0	0,0		100	0	

*negative values set to zero for the calculation of percentage distribution.

Table D3:

Extraction time 5 hours	^{134}Cs						^{137}Cs					
	DPM			Percentage distribution			DPM			Percentage distribution		
Sample – *PSU* value	DPM LMM	DPM HMM	DPM >0.45 *µm*	% distribution LMM	% distribution HMM*	% distribution >0.45 *µm*	DPM LMM	DPM HMM	DPM >0.45 *µm*	% distribution LMM	% distribution HMM*	% distribution >0.45 *µm*
1-1	464,9	0,0	0,0	100	0	0	743,8	3,8	32,3	95	0	4
1-2	386,0	0,0	0,0	100	0	0	754,3	0,0	24,7	97	0	3
1-3	348,2	0,0	22,7	94	0	6	735,2	0,0	23,9	97	0	3
3-1	318,4	0,0	0,0	100	0	0	734,1	0,0	27,4	96	0	4
3-2	365,6	0,0	0,0	100	0	0	712,2	0,0	20,3	97	0	3
3-3	376,2	0,0	12,0	97	0	3	780,1	0,0	21,3	97	0	3
5-1	352,5	0,0	16,4	96	0	4	772,6	0,0	18,8	98	0	2
5-2	427,5	0,0	20,2	95	0	5	728,3	3,1	27,6	96	0	4
5-3	347,5	0,0	1,8	99	0	1	705,9	5,0	19,1	97	1	3
10-1	420,7	0,0	2,2	99	0	1	742,8	33,1	26,4	93	4	3
10-2	451,6	4,7	0,0	99	1	0	764,4	0,0	21,6	97	0	3
10-3	376,4	0,0	0,0	100	0	0	723,6	0,0	13,3	98	0	2
15-1	391,3	0,0	0,0	100	0	0	733,8	0,0	16,8	98	0	2
15-2	413,1	0,0	5,1	99	0	1	715,7	0,0	21,9	97	0	3
15-3	374,5	0,0	9,6	97	0	3	688,1	0,0	21,3	97	0	3
25-1	400,2	0,0	7,5	98	0	2	764,3	0,0	15,7	98	0	2
25-2	451,5	0,0	5,6	99	0	1	750,8	0,0	20,8	97	0	3
25-3	460,4	0,0	0,0	100	0	0	717,2	0,0	22,9	97	0	3

*negative values set to zero for the calculation of percentage distribution.

Table D4:

Extraction time 24 hours	^{134}Cs						^{137}Cs					
	DPM			Percentage distribution			DPM			Percentage distribution		
Sample – *PSU* value	DPM LMM	DPM HMM	DPM >0.45 *µm*	% distribution LMM	% distribution HMM*	% distribution >0.45 *µm*	DPM LMM	DPM HMM	DPM >0.45 *µm*	% distribution LMM	% distribution HMM*	% distribution >0.45 *µm*
1-1	373,1	0,0	12,4	97	0	3	731,1	0,0	22,4	97	0	3
1-2	404,7	0,0	0,0	100	0	0	767,4	0,0	19,2	98	0	2
1-3	426,4	0,0	36,2	92	0	8	774,6	0,0	21,1	97	0	3
3-1	329,6	0,0	18,4	95	0	5	749,2	0,0	14,8	98	0	2
3-2	372,0	0,0	9,3	98	0	2	747,9	0,0	22,1	97	0	3
3-3	378,7	0,0	6,9	98	0	2	749,9	0,0	24,8	97	0	3
5-1	334,5	0,0	35,3	90	0	10	756,4	0,0	16,6	98	0	2
5-2	445,3	0,0	22,7	95	0	5	725,4	0,0	18,6	98	0	2
5-3	359,1	0,0	18,4	95	0	5	704,9	0,0	16,6	98	0	2
10-1	369,8	0,0	0,0	100	0	0	731,1	0,0	23,5	97	0	3
10-2	429,5	0,0	9,1	98	0	2	782,7	0,0	17,9	98	0	2
10-3	405,6	0,0	0,0	100	0	0	729,4	0,0	18,0	98	0	2
15-1	346,7	0,0	6,0	98	0	2	766,2	0,0	29,4	96	0	4
15-2	375,8	0,0	13,6	96	0	4	748,1	0,0	8,1	99	0	1
15-3	343,6	0,0	19,8	95	0	5	741,5	0,0	23,4	97	0	3
25-1	427,6	0,0	1,3	100	0	0	743,8	0,0	23,7	97	0	3
25-2	467,8	0,0	26,5	95	0	5	733,9	0,0	20,0	97	0	3
25-3	450,0	0,0	15,6	97	0	3	737,2	0,0	20,8	97	0	3

*negative values set to zero for the calculation of percentage distribution.

Table D5:

Extraction time 8 days	^{134}Cs						^{137}Cs					
	DPM			Percentage distribution			DPM			Percentage distribution		
Sample – *PSU* value	DPM LMM	DPM HMM	DPM >0.45 *µm*	% distribution LMM	% distribution HMM*	% distribution >0.45 *µm*	DPM LMM	DPM HMM	DPM >0.45 *µm*	% distribution LMM	% distribution HMM*	% distribution >0.45 *µm*
1-1	454,0	5,8	52,7	89	1	10	786,4	7,6	32	95	1	4
1-2	438,0	42,4	10,5	89	9	2	755,4	3,4	25	96	0	3
1-3	436,0	0,0	40,5	91	0	9	770,1	5,2	24	96	1	3
3-1	309,8	0,0	2,4	99	0	1	763,2	3,6	27	96	0	3
3-2	425,1	0,0	31,5	93	0	7	770,4	10,4	20	96	1	3
3-3	376,7	0,0	13,5	97	0	3	727,8	8,1	21	96	1	3
5-1	395,3	14,0	38,7	88	3	9	752,9	2,2	19	97	0	2
5-2	481,6	0,0	20,7	96	0	4	750,3	4,3	28	96	1	4
5-3	437,5	7,5	27,8	93	2	6	738,8	5,5	19	97	1	3
10-1	462,7	13,6	0,0	97	3	0	784,5	9,3	26	96	1	3
10-2	419,3	6,4	22,4	94	1	5	755,7	7,8	22	96	1	3
10-3	476,7	4,2	0,0	99	1	0	823,2	7,4	13	98	1	2
15-1	383,5	16,0	21,6	91	4	5	749,7	6,1	17	97	1	2
15-2	468,7	10,4	2,9	97	2	1	764,8	9,6	22	96	1	3
15-3	430,2	20,7	0,0	95	5	0	772,8	-0,5	21	97	0	3
25-1	484,7	11,1	35,3	91	2	7	768,9	7,3	16	97	1	2
25-2	503,3	29,6	30,4	89	5	5	776,6	3,7	21	97	0	3
25-3	479,8	10,4	26,2	93	2	5	744,1	7,8	23	96	1	3

*negative values set to zero for the calculation of percentage distribution.

Table D6:

Extraction time 1 months	^{134}Cs						^{137}Cs					
	DPM			Percentage distribution			DPM			Percentage distribution		
Sample – *PSU* value	DPM LMM	DPM HMM	DPM >0.45 *µm*	% distribution LMM	% distribution HMM*	% distribution >0.45 *µm*	DPM LMM	DPM HMM	DPM >0.45 *µm*	% distribution LMM	% distribution HMM*	% distribution >0.45 *µm*
1-1	388,7	0,0	61,5	86	0	14	678,2	9,3	18,9	96	1	3
1-2	397,1	0,0	28,4	93	0	7	716,1	5,8	14,9	97	1	2
1-3	310,4	26,2	0,0	92	8	0	754,8	4,6	23,6	96	1	3
3-1	318,2	5,3	0,0	98	2	0	720,9	10,4	20,6	96	1	3
3-2	429,8	2,9	0,0	99	1	0	740,9	4,1	21,7	97	1	3
3-3	348,0	9,6	0,0	97	3	0	729,2	7,0	30,6	95	1	4
5-1	346,2	0,0	0,0	100	0	0	709,6	9,4	17,7	96	1	2
5-2	366,9	48,9	3,1	88	12	1	725,4	5,6	26,0	96	1	3
5-3	454,5	0,0	6,7	99	0	1	685,0	10,3	20,3	96	1	3
10-1	434,0	51,1	0,0	89	11	0	726,6	11,2	19,9	96	1	3
10-2	407,6	26,4	22,5	89	6	5	710,5	1,6	19,8	97	0	3
10-3	350,2	36,7	41,8	82	9	10	756,3	9,9	25,3	96	1	3
15-1	327,3	4,4	8,7	96	1	3	727,4	8,3	27,6	95	1	4
15-2	370,0	0,0	8,4	98	0	2	749,4	4,0	20,1	97	1	3
15-3	325,6	45,1	44,0	79	11	11	706,9	10,8	9,9	97	1	1
25-1	459,6	34,5	0,0	93	7	0	709,6	4,8	21,3	96	1	3
25-2	392,4	2,9	35,8	91	1	8	683,4	9,3	13,3	97	1	2
25-3	392,7	10,5	0,0	97	3	0	725,3	1,1	23,8	97	0	3

*negative values set to zero for the calculation of percentage distribution.

9.5 Appendix E – Clay content

Table E1: Results from determining gram clay per liter by pipetting 1 ml of the clay suspension, drying (60◦C) and determining weight with an analytical balance (Accuracy 0.0001 g).

Sample (1 ml)	Clay (g)
1	0,0065
2	0,0070
3	0,0069
Average	0,0068

9.6 Appendix F: Distribution coefficient, K_d

Table F1: Apparent distribution coefficient for ^{134}Cs and ^{137}Cs at salinity 1 *PSU*.

K_d		Hours					
	1 *PSU*	0,5	2	5	24	192	720
Cs-134 DPM/kg >0.45 *um* / Cs-134 DPM/L LMM	K_d Cs-134	701	410	328	219	226	215
Cs-137 DPM/Kg >0.45 *um* / CS-137 DPM/L LMM	K_d Cs-137	31	45	61	78	128	161

Table F2: Apparent distribution coefficient for ^{134}Cs and ^{137}Cs at salinity 3 *PSU*.

K_d		Hours					
	3 *PSU*	0,5	2	5	24	192	720
Cs-134 DPM/kg >0.45 *um* / Cs-134 DPM/L LMM	K_d Cs-134	441	354	267	208	188	147
Cs-137 DPM/kg >0.45 *um* / CS-137 DPM/L LMM	K_d Cs-137	28	27	38	52	88	84

Table F3: Apparent distribution coefficient for ^{134}Cs and ^{137}Cs at salinity 5 *PSU*.

K_d		Hours					
	5 *PSU*	0,5	2	5	24	192	720
Cs-134 DPM/kg >0.45 *um* / Cs-134 DPM/L LMM	K_d Cs-134	427	333	236	204	173	150
Cs-137 DPM/kg >0.45 *um* / CS-137 DPM/L LMM	K_d Cs-137	17	23	25	41	70	79

Table F4: Apparent distribution coefficient for ^{134}Cs and ^{137}Cs at salinity 10 *PSU*.

K_d		Hours					
	10 *PSU*	0,5	2	5	24	192	720
Cs-134 DPM/kg >0.45 *um* / Cs-134 DPM/L LMM	K_d Cs-134	369	268	197	182	141	107
Cs-137 DPM/kg >0.45 *um* / CS-137 DPM/L LMM	K_d Cs-137	12	16	16	25	39	47

Table F5: Apparent distribution coefficient for ^{134}Cs and ^{137}Cs at salinity 15 *PSU*.

K_d		Hours					
	15 *PSU*	0,5	2	5	24	192	720
Cs-134 DPM/kg >0.45 *um* / Cs-134 DPM/L LMM	K_d Cs-134	322	285	266	172	148	99
Cs-137 DPM/kg >0.45 *um* / CS-137 DPM/L LMM	K_d Cs-137	8	11	14	19	29	29

Table F6: Apparent distribution coefficient for ^{134}Cs and ^{137}Cs at salinity 25 *PSU*.

K_d		Hours					
	25 *PSU*	0,5	2	5	24	192	720
Cs-134 DPM/kg >0.45 *um* / Cs-134 DPM/L LMM	K_d Cs-134	390	309	224	155	131	73
Cs-137 DPM/kg >0.45 *um* / CS-137 DPM/L LMM	K_d Cs-137	7	10	10	14	19	13

9.7 Appendix G: - Determination of transformation rates

Determination of transformation rates from sorption and desorption measurements

Magne Simonsen, Øyvind Saetra

April 29, 2019

1 Derivation of equations

We assume that the ^{137}Cs and ^{134}Cs radionuclides can be present in two physico-chemical forms; LMM (dissolved in aquatic solution) and solid (bound to particles or sediments). The total radionuclide concentration is assumed to be constant, i.e., the system is closed with no sources and sinks, and the total concentration can be divided into the LMM fraction, C_w, and the solid fraction, C_s.

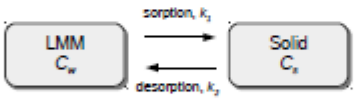

Figure 1: Sketch of the model system.

The transformation processes are assumed to affect the fractions with constant transfer rates, k_1 and k_2, describing the desorption and sorption, respectively, as sketched in Fig 1. The processes are assumed to be reversible, and may be described by the following equations:

$$\frac{\mathrm{d}C_w}{\mathrm{d}t} = -k_1 C_w + k_2 C_s \tag{1}$$

$$\frac{\mathrm{d}C_s}{\mathrm{d}t} = k_1 C_w - k_2 C_s \tag{2}$$

Summing (1) and 2, it follows that

$$C_s + C_w = 1 \tag{3}$$

and hence, if we assume that these equations describe the involved processes properly, the total radionuclide content must be constant in our closed system.

Combining (1) with (3) and introducing

$$\alpha = k_1 + k_2 \tag{4}$$

and

$$\beta = \frac{k_2}{k_1 + k_2}, \tag{5}$$

we get

$$\frac{\mathrm{d}C_w}{\mathrm{d}t} = -\alpha(C_w - \beta). \tag{6}$$

By integrating from $t = 0$ to t, this differential equation can be solved as

$$\int_{C_{w0}}^{C_w} \frac{\mathrm{d}C_w}{C_w - \beta} = -\int_0^t \alpha \mathrm{d}t \tag{7}$$

giving

$$\ln\left(\frac{C_w - \beta}{C_{w0} - \beta}\right) = -\alpha t \tag{8}$$

which can be further transformed to

$$C_w = (C_{w0} - \beta)e^{-\alpha t} + \beta \tag{9}$$

where C_{w0} is the initial LMM fraction (C_w at $t = 0$).

Under equilibrium conditions ($t \to \infty$), (1) turns into

$$0 = -k_1 C_w + k_2 C_s, \tag{10}$$

giving

$$\frac{k_1}{k_2} = \frac{C_{se}}{C_{we}} \equiv K_d \tag{11}$$

where C_{se} and C_{we} are the equilibrium fractions of solid and LMM species, respectively, and K_d is the distribution coefficient[1].

Setting ($t \to \infty$) into (9) gives

$$C_{we} = \beta \tag{12}$$

and thus, equation (8) and (9) can be rewritten as

$$\ln\left(\frac{C_w - C_{we}}{C_{w0} - C_{we}}\right) = -\alpha t \tag{13}$$

and

$$C_w(t) = (C_{w0} - C_{we})e^{-\alpha t} + C_{we}. \tag{14}$$

[1] Note that this definition of the distribution coefficient K_d refers to the fractions associated to solid and dissolved matter in percent of the total activity, respectively, not to the absolute concentrations.

2 Application of data from the sorption experiments

Now, to estimate α, a curve was fitted to the slope of the experimentally obtained C_w values in (13). The measurements taken at the two latest time steps ($t = 192$h and $t = 720$h) were omitted. When we know α, we can estimate the transfer rates k_1 and k_2 by using (11):

$$k_1 = \frac{\alpha}{1 + 1/K_d} \tag{15}$$

$$k_2 = \frac{k_1}{K_d}. \tag{16}$$

Curves of the values obtained by (13) are plotted in Fig 2, including slopes (α) estimated by the least square method. The equilibrium values (C_{we}) were set to the C_w value at the latest time step, adjusted with 1 % to avoid singularity. The initial values (C_{w0}) were set to the values at $t = 0$ (100 % in this case).

The experimentally obtained k_1, k_2 and K_d values are shown in Table 1.

Using these estimated transfer rates (Table 1) in equation (14) gives the analytically estimated curves for C_w, while the C_s curves were obtained from (3). These functions are plotted in Fig 3.

The k_1, k_2 and K_d values obtained from the sorption experiments at the different salinities are plotted in Fig 4.

Table 1: The estimated transfer rates and K_d values from the ^{137}Cs sorption data. Unit of the salinity is PSU, units of the transfer rates are s^{-1}, while K_d is dimensionless.

Sal	k_1	k_2	K_d
1	4.448×10^{-6}	3.771×10^{-6}	1.180
3	3.804×10^{-6}	6.069×10^{-6}	0.627
5	3.124×10^{-6}	5.217×10^{-6}	0.599
10	1.734×10^{-6}	4.872×10^{-6}	0.356
15	1.452×10^{-6}	6.608×10^{-6}	0.220
25	1.717×10^{-6}	1.777×10^{-5}	0.097

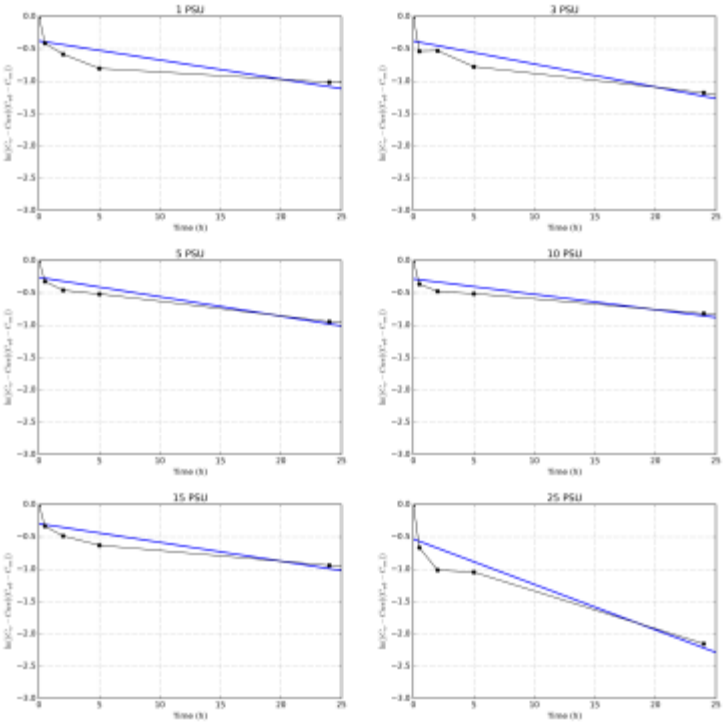

Figure 2: Estimated slopes (blue lines) of the values of equation (13) (black points) using C_w values obtained from the sorption experiments at different salinities.

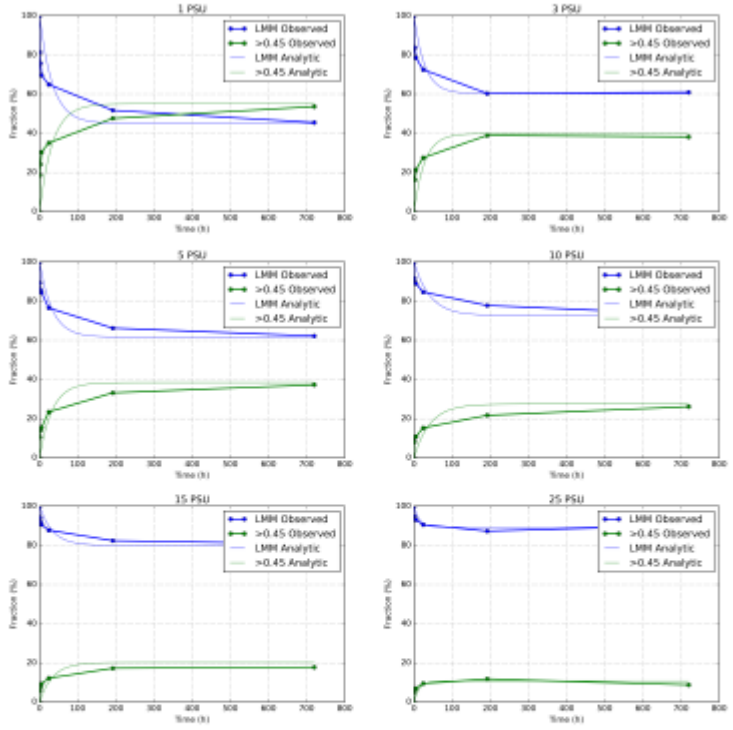

Figure 3: Estimated and measured fractions of LMM (blue points/lines) and solid (green points/lines) species from the ^{137}Cs sorption experiments.

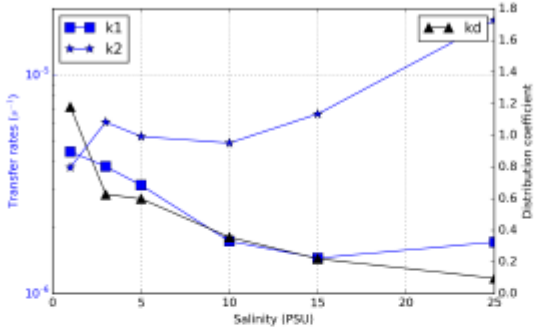

Figure 4: The transfer rates (on the left-hand log-scale y-axis) and K_d values (on the right-hand linear y-axis) obtained from the ^{137}Cs sorption experiments.

3 Application of data from the desorption experiments

Similarly to the results from the sorption experiments, values from the ^{134}Cs desorption experiments were used to calculate the transfer rates. The estimated slopes are plotted in Fig 5.

The concentration fractions obtained from desorption experiments as well as the analytically estimated curves are plotted in Fig 6.

The experimentally obtained k_1, k_2 and K_d values are shown in Table 2.

The k_1, k_2 and K_d values obtained from the desorption experiments at the different salinities are plotted in Fig 7.

Table 2: The estimated transfer rates and K_d values from the ^{134}Cs desorption data. Unit of the salinity is PSU, units of the transfer rates are s^{-1}, while K_d is dimensionless.

Sal	k_1	k_2	K_d
1	-	-	1.736
3	7.354×10^{-6}	6.679×10^{-6}	1.101
5	8.331×10^{-6}	7.462×10^{-6}	1.116
10	5.742×10^{-6}	7.056×10^{-6}	0.814
15	5.217×10^{-6}	6.964×10^{-6}	0.749
25	4.174×10^{-6}	7.623×10^{-6}	0.548

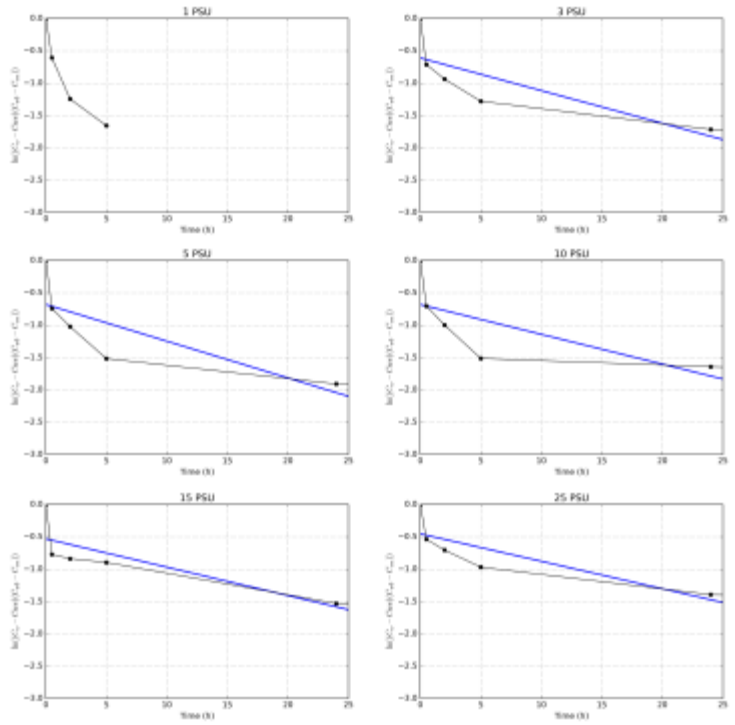

Figure 5: Estimated slopes (blue lines) of the values of equation (13) (black points) using C_w values obtained from the desorption experiments at different salinities. Note that in the 1 PSU plot, the slope, and hence the transfer rates. could not be estimated with equation (13) due singularity caused by negative values in the logarithmic expression.

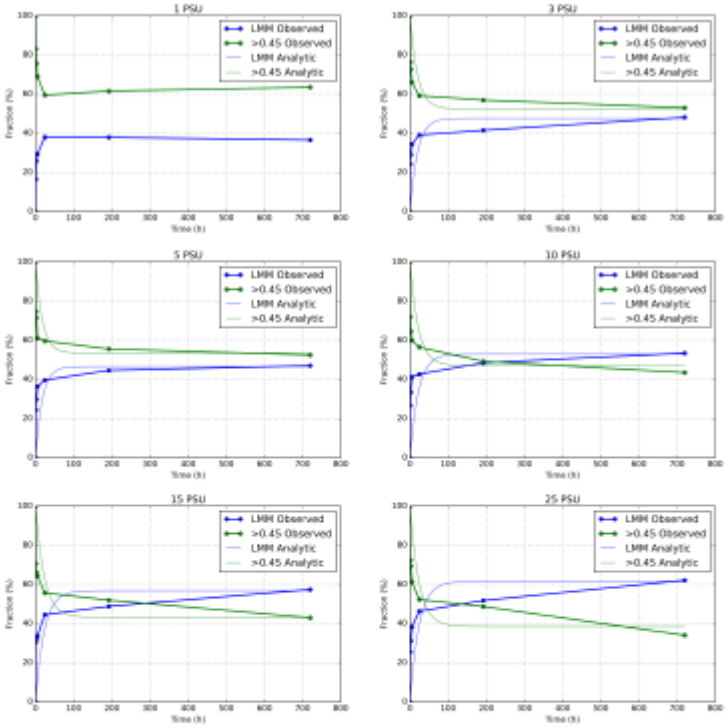

Figure 6: Estimated and measured fractions of LMM (blue points/lines) and solid (green points/lines) species.

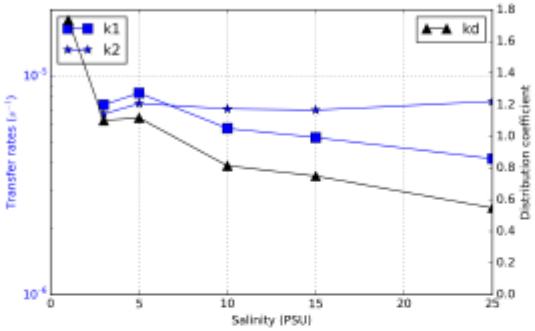

Figure 7: The transfer rates (on the left-hand log-scale y-axis) and K_d values (on the right-hand linear y-axis) obtained from the ^{134}Cs desorption experiments.

Norges miljø- og biovitenskapelige universitet
Noregs miljø- og biovitskapelege universitet
Norwegian University of Life Sciences

Postboks 5003
NO-1432 Ås
Norway